



**NAVAL  
POSTGRADUATE  
SCHOOL**

**MONTEREY, CALIFORNIA**

**THESIS**

**STRUCTURE AND DYNAMICS OF THE THERMOHALINE  
STAIRCASES IN THE BEAUFORT GYRE**

by

Ana Lisa Wilson

September 2007

Thesis Advisor:  
Second Reader:

Timour Radko  
John Colosi

**Approved for public release; distribution is unlimited**

THIS PAGE INTENTIONALLY LEFT BLANK

<b>REPORT DOCUMENTATION PAGE</b>			Form Approved OMB No. 0704-0188	
Public reporting burden for this collection of information is estimated to average 1 hour per response, including the time for reviewing instruction, searching existing data sources, gathering and maintaining the data needed, and completing and reviewing the collection of information. Send comments regarding this burden estimate or any other aspect of this collection of information, including suggestions for reducing this burden, to Washington headquarters Services, Directorate for Information Operations and Reports, 1215 Jefferson Davis Highway, Suite 1204, Arlington, VA 22202-4302, and to the Office of Management and Budget, Paperwork Reduction Project (0704-0188) Washington DC 20503.				
<b>1. AGENCY USE ONLY (Leave blank)</b>		<b>2. REPORT DATE</b> September 2007	<b>3. REPORT TYPE AND DATES COVERED</b> Master's Thesis	
<b>4. TITLE AND SUBTITLE</b> Structure and Dynamics of the Thermohaline Staircases in the Beaufort Gyre			<b>5. FUNDING NUMBERS</b>	
<b>6. AUTHOR(S)</b> Ana Lisa Wilson				
<b>7. PERFORMING ORGANIZATION NAME(S) AND ADDRESS(ES)</b> Naval Postgraduate School Monterey, CA 93943-5000			<b>8. PERFORMING ORGANIZATION REPORT NUMBER</b>	
<b>9. SPONSORING /MONITORING AGENCY NAME(S) AND ADDRESS(ES)</b>			<b>10. SPONSORING/MONITORING AGENCY REPORT NUMBER</b>	
<b>11. SUPPLEMENTARY NOTES</b> The views expressed in this thesis are those of the author and do not reflect the official policy or position of the Department of Defense or the U.S. Government.				
<b>12a. DISTRIBUTION / AVAILABILITY STATEMENT</b> Approved for public release; distribution is unlimited			<b>12b. DISTRIBUTION CODE</b>	
<b>13. ABSTRACT (maximum 200 words)</b> <p>This study explores the dynamics of diffusive convection which occurs when cold, fresh water overlies warm and salty. The primary convective regime in the Arctic region is characterized by the spontaneous formation of well mixed layers separated by thin high-gradient interfaces known as thermohaline staircases.</p> <p>Data analysis and analytical considerations are used to estimate the vertical heat/salt mixing rates and their dependencies on the large-scale environmental parameters. Based on the analysis of Beaufort staircases, we suggest that the layer thickness, as well as the vertical heat/salt fluxes, is controlled by the patterns of merging events in which relatively small steps are systematically eliminated. Significant concerns are raised with regard to the direct extrapolation of laboratory derived flux laws to ocean conditions. An alternative method of analysis is proposed which involves recalibration of the laboratory-derived flux laws for the oceanic conditions.</p> <p>Extrapolated diffusive convective fluxes are in the range of <math>1-6 \text{ Wm}^{-2}</math>, comparable to magnitude of fluxes currently unaccounted for in the Arctic heat budget. We propose that the parameterizations of the diffusive fluxes in thermohaline staircases can be used to enhance understanding of Arctic climate changes and predictive capabilities of large-scale numerical models. Preliminary findings are indicative of the importance of diffusive convection for sound propagation in the Arctic region - the problem of great interest for various Naval research applications in the area.</p>				
<b>14. SUBJECT TERMS</b> Diffusive Convection, Arctic Staircases, diffusive fluxes, diffusive layering.			<b>15. NUMBER OF PAGES</b> 77	
			<b>16. PRICE CODE</b>	
<b>17. SECURITY CLASSIFICATION OF REPORT</b> Unclassified	<b>18. SECURITY CLASSIFICATION OF THIS PAGE</b> Unclassified	<b>19. SECURITY CLASSIFICATION OF ABSTRACT</b> Unclassified	<b>20. LIMITATION OF ABSTRACT</b> UU	

THIS PAGE INTENTIONALLY LEFT BLANK

**Approved for public release; distribution is unlimited**

**STRUCTURE AND DYNAMICS OF THE THERMOHALINE STAIRCASES IN THE  
BEAUFORT GYRE**

Ana L. Wilson  
Lieutenant, United States Navy  
B.S., United States Naval Academy 2000

Submitted in partial fulfillment of the  
requirements for the degree of

**MASTER OF SCIENCE IN METEOROLOGY AND PHYSICAL OCEANOGRAPHY**

from the

**NAVAL POSTGRADUATE SCHOOL  
September 2007**

Author: Ana Lisa Wilson

Approved by: Timour Radko  
Thesis Advisor

John Colosi  
Second Reader

Mary L. Batteen  
Chairman, Department of Oceanography

THIS PAGE INTENTIONALLY LEFT BLANK

## ABSTRACT

This study explores the dynamics of diffusive convection which occurs when cold, fresh water overlies warm and salty water. Diffusive convection is generally observed in high-latitude regions, particularly in the Arctic Ocean, between the base of the mixed layer and the top of the Atlantic water. The primary convective regime in this region is characterized by the spontaneous formation of well mixed layers separated by thin high-gradient interfaces known as thermohaline staircases.

Data analysis and analytical considerations are used to estimate the vertical heat/salt mixing rates and their dependencies on the large-scale environmental parameters. The ice-tethered profiler data from the Beaufort Gyre are analyzed to determine the origin of the thermohaline staircases and the mechanism for selection of the preferred layer thickness. Based on the analysis of Beaufort staircases, we suggest that the layer thickness, as well as the vertical heat/salt fluxes, is controlled by the patterns of merging events in which relatively small steps are systematically eliminated. Significant concerns are raised with regard to the direct extrapolation of laboratory derived flux laws to ocean conditions – a conventional approach to the analysis of the Arctic staircases. An alternative and more accurate method of analysis is proposed which involves recalibration of the laboratory-derived flux laws for the oceanic conditions.

Extrapolated diffusive convective fluxes are in the range of  $1-6 \text{ Wm}^{-2}$ , which is comparable to magnitude of

fluxes currently unaccounted for in the Arctic heat budget. We propose that the parameterizations of the diffusive fluxes in thermohaline staircases, developed in this thesis, can be used to enhance understanding of Arctic climate changes and predictive capabilities of large-scale numerical models. Preliminary findings are indicative of the importance of diffusive convection for sound propagation in the Arctic region – the problem of great interest for various Naval research applications in the area.

## TABLE OF CONTENTS

I.	INTRODUCTION .....	1
A.	DOUBLE DIFFUSION .....	1
1.	Salt Fingers .....	2
2.	Diffusive Convection .....	3
B.	THEORETICAL BACKGROUND .....	10
C.	ICE-TETHERED PROFILER .....	13
II.	CHARACTERISTICS OF THERMOHALINE STAIRCASES .....	17
A.	STEADY CHARACTERISTICS .....	17
B.	EVOLUTIONARY PATTERN .....	27
III.	MERGING THEOREM FOR A TWO COMPONENT FLUID .....	29
IV.	APPLICATIONS OF THE MERGING THEOREM TO OCEANIC DATA ....	37
V.	ACOUSTIC APPLICATIONS .....	45
A.	EFFECTS OF THERMOHALINE STEPS ON ACOUSTIC TRANSMISSION .....	45
B.	INITIAL APPLICATION TO DIFFUSIVE CONVECTION .....	45
C.	THE ARCTIC CASE .....	47
VI.	CONCLUSIONS .....	53
	LIST OF REFERENCES .....	55
	INITIAL DISTRIBUTION LIST .....	59

THIS PAGE INTENTIONALLY LEFT BLANK

## LIST OF FIGURES

Figure 1.	Simplified diagram of ocean double diffusive regimes. a) Salt Finger Regime b) Diffusive Convection Regime.....	2
Figure 2.	Laboratory simulation of salt fingers. The magenta plumes are salty water pushing into the colder fresher water. (From University of Alaska Fairbanks website, <a href="http://www.ims.uaf.edu">www.ims.uaf.edu</a> ).....	3
Figure 3.	Basic set-up of diffusive layers.....	4
Figure 4.	Physical mechanism behind diffusive layering.....	5
Figure 5.	Regions susceptible to double diffusion. The light grey areas indicate where density ratio is from 3-10. Dark grey indicates $1 \leq R_\rho < 3$ . The red circle indicates the Beaufort Gyre.....	6
Figure 6.	Arctic circulation pattern, resulting in conditions favorable for diffusive convection. (Illustration by Jack Cook, Woods Hole Oceanographic Institution.).....	7
Figure 7.	Cross section of Arctic water mass. Cold, fresh water overlies warm, salty Atlantic water. (Illustration by Jayne Doucette, Woods Hole Oceanographic Institute.).....	8
Figure 8.	Side view of diffusive layering created by heating a salt gradient from below, after Figure 6 (Kelley 2003) A is the first quasi-stationary interface. B is the secondary interface, forming above it.....	9
Figure 9.	A series of convecting layers and heat-salt diffusive interfaces (Turner 1968).....	9
Figure 10.	Buoyancy flux ratio $R_f(R_\rho)$ for diffusive convection in the laboratory. Data from three different laboratory sources Crapper (1975), Turner (1965), and Newell (1984) from Kelley (1990). The solid line is the empirical fit....	12
Figure 11.	Schematic of Ice-Tethered Profiler (Krishfield et al., 2006).....	14
Figure 12.	ITP 1 and ITP 3 drift tracks. (a) Drift track for ITP 1 and (b) is ITP3 drift track. From Woods Hole Oceanographic Institute Ice Tethered Profiler site ( <a href="http://www.whoi.edu/itp/data.html">http://www.whoi.edu/itp/data.html</a> ).....	15
Figure 13.	Temperature Depth Profile. The section of the profile is highlighted. H calculations are	

	determined from the midpoint of each staircase depth.....	18
Figure 14.	Salinity depth profile. Same location as previous figure. (Salinity is calculated using MATLAB polyfit to de-spike data).....	19
Figure 15.	Non dimensional $\alpha\Delta T$ is plotted as a function of layer thickness, H (meters).....	21
Figure 16.	Non-dimensional $\beta\Delta S$ is plotted as a function of layer thickness H (meters).....	22
Figure 17.	Comparison of $\alpha\Delta T$ and $R_\rho$ using average data from September 2005 to October 2006.....	23
Figure 18.	Comparison of $\beta\Delta S$ and $R_\rho$ using average data from September 2005 to October 2006.....	24
Figure 19.	Comparison of density ratios over the interface and density ratios over the step.....	25
Figure 20.	Examples of merging events, as seen from the inspection of the conductivity data.....	27
Figure 21.	Temperature variation in time. Each data point represents temperature on a particular profile..	28
Figure 22.	Schematic of H-merger evolution in time.....	29
Figure 23.	Schematic of B-merger evolution in time.....	30
Figure 24.	Schematic diagram illustrating the stability analysis for an infinite series of interfaces. (a) Basic state consisting of identical steps. (b) Perturbed state in which the T,S jumps at the even interfaces are slightly decreased, and the jumps at odd interfaces are increased.....	32
Figure 25.	Change in temperature vs. time during the merging period. The normalized growth rate for this merger is 4.7E-04 and the density ratio is 2.8631.....	38
Figure 26.	Change in temperature vs. during the merging period. The normalized growth rate for this merger is 8.6E-04 and the density ratio is 2.4035.....	39
Figure 27.	Using the coefficient A=30, theoretical data fits Beaufort Gyre data within 95% prediction bounds.....	40
Figure 28.	Using the coefficient A=15.75 applied to Marmorino and Caldwell (1976), theoretical data fits Beaufort Gyre data within 95% prediction bounds.....	41
Figure 29.	a) Typical temperature and salinity plot for salt finger region. Salinity, Potential Temperature and Density plots show thermohaline	

	step characteristics.      b) Sound velocity profiles showing the step data, standard depth profiles and historical averaged sound velocity profile data. From Chin-Bing et al. (1994).....	46
Figure 30.	Temperature and depth profile used for acoustic simulation.....	48
Figure 31.	Sound Velocity Profile from ITP 1 raw1013 data. Red profile smoothes staircase structure, blue includes staircases. The graphic on the right is an enhancement to the SVP so that the staircase region is more visible.....	49
Figure 32.	Sound propagation through SVP with no staircases.....	50
Figure 33.	Sound Propagation model through SVP with staircase structure included.....	51
Figure 34.	Difference in TL between profiles with and without staircases.....	52

THIS PAGE INTENTIONALLY LEFT BLANK

## LIST OF TABLES

Table 1.	Average data from ITP 1 and ITP 3 by month and over the entire data set.....	20
Table 2.	Data comparison of calculated normalized growth rate from actual data and the normalized growth rates using a constant factor with the $4/3$ flux law.....	41
Table 3.	ITP 1 data for April 2006 in 20-40 meter layer increments.....	42
Table 4.	Heat Fluxes in the Beaufort Gyre using the calibrated flux laws.....	43

THIS PAGE INTENTIONALLY LEFT BLANK

## ACKNOWLEDGMENTS

I would like to express many thanks to Dr. Timour Radko for his advice, support, patience, and expertise in completing the thesis process. Many thanks go to Dr. John Toole, Dr. Laurie Padman, and Dr. Dan Kelley, who were more than willing to give their advice and opinions. I would also like to thank Commander Ben Reeder, USN, for his help in the acoustic portion of this thesis, and Dr. John Colosi, who believed that the acoustic portion was worth looking into.

Much gratitude is also to be expressed to Mike Cook, whose MATLAB expertise saved my thesis many times, and without whom I would still be calculating by hand. The rest of the NPS faculty has been extremely helpful and provided guidance in many ways during my tenure at Naval Postgraduate School, and I appreciate it greatly.

Finally, I would like to thank my friends and family who know very little of double diffusion, yet patiently listened and supported me through it all.

THIS PAGE INTENTIONALLY LEFT BLANK

## **I. INTRODUCTION**

The polar ice cap, consistently regarded as a hindrance to data collection in the Arctic, is currently under-sampled. With evidence of increasing Arctic temperatures and decreasing sea-ice thickness, the need to parameterize unresolved ocean processes, and include them in climate models, is becoming a necessity. This study focuses on the double diffusive region of the Beaufort Gyre.

### **A. DOUBLE DIFFUSION**

Before discussing the Arctic data, the basic concepts behind double diffusion should be reviewed. Although double diffusion occurs in many different systems, it has a vast impact on ocean dynamics. Turner (1973) provided an entire chapter on the dynamics of double diffusive regimes in his book on the buoyancy effects in fluids. He describes double-diffusion as the process related to the presence of more than one component contributing to the density of the ocean with different molecular diffusivities. In the ocean case, the dominant density components are temperature and salinity. Ocean double diffusion takes two forms. The most studied is the salt finger regime, where warm, salty water lies above cold, fresh water. The other regime, which is the focus of this study, is diffusive convection where cold, fresh water overlies warm, salty water. Stratification patterns which support salt-fingering and diffusive convection are shown in the schematic diagrams in Figure 1.

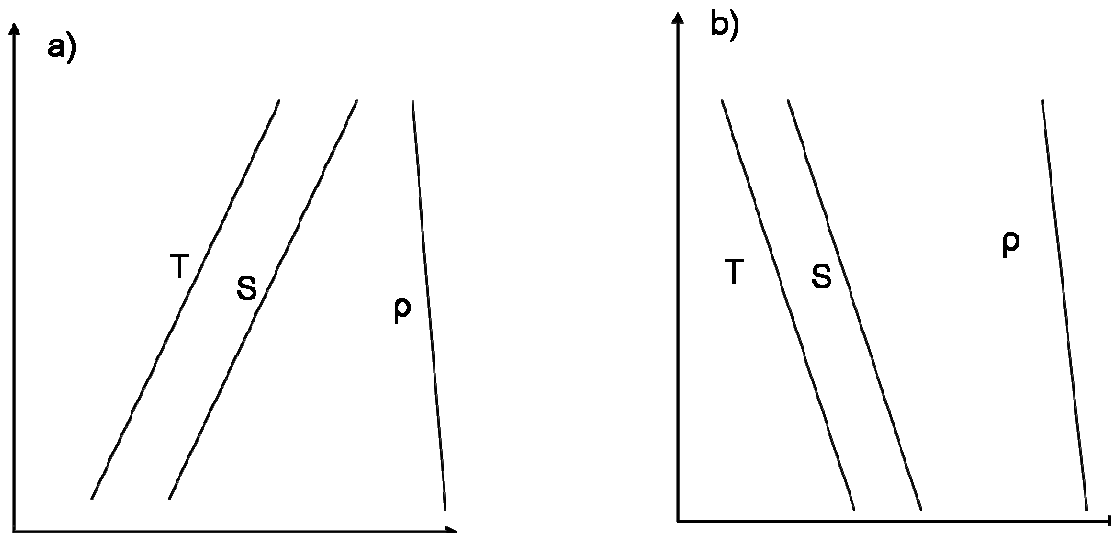


Figure 1. Simplified diagram of ocean double diffusive regimes. a) Salt Finger Regime b) Diffusive Convection Regime.

## 1. Salt Fingers

The majority of research has focused on the salt-fingering regime. Stommel et al. (1956) brought interest to the salt finger regime by hypothesizing that by exploiting the warm, salty water over cooler, fresher water, an energy source termed "the perpetual salt fountain" could be formed. The concept being that a thin membrane in the shape of a tube could allow temperature diffusion, but not salinity diffusion, and create an energy source by making a parcel of salty water rise as it tries to reach a state of equilibrium. While the proposed idea has yet to be fully developed in the ocean, the interest in salt fingering made its debut.

Stern (1960) described salt-fingers as instabilities that arise when relatively warm, salty water lies over colder, fresher water of a higher density and consists of

long fingers of rising and sinking water. The warmer, salty water rapidly loses heat while retaining its salinity. The increasing parcel density makes it sink further, drawing more warm, salty water from above, resulting in the fingers of salty fluid. Figure 2 shows the resulting salt fingers. In this case the magenta dye is applied to the warm, salty water.



Figure 2. Laboratory simulation of salt fingers. The magenta plumes are salty water pushing into the colder fresher water. (From University of Alaska Fairbanks website, [www.ims.uaf.edu](http://www.ims.uaf.edu)).

## **2. Diffusive Convection**

The dynamics of double-diffusive convection differ substantially from those of salt fingering. Diffusive convection occurs in both a smooth gradient region and a

stepped configuration, which is more common in nature (Figure 3). For the diffusive convection case, relatively cold, fresh water overlies warm, salty water with a thin interface in between.

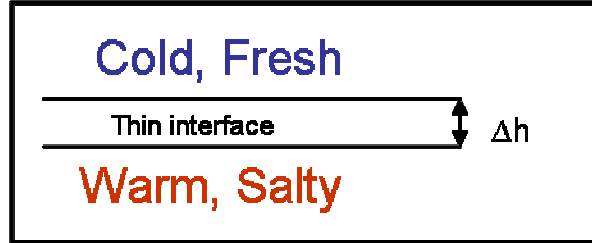


Figure 3. Basic set-up of diffusive layers.

Molecular fluxes across the interface are:

$\alpha F_{TM} = \kappa_T \frac{\alpha \Delta T}{\Delta h}$  and  $\beta F_{SM} = \kappa_S \frac{\beta \Delta S}{\Delta h}$  where  $\alpha$  is the coefficient of volume expansion due to unit temperature change,  $\beta$  is the proportional density change produced by unit density salinity change,  $F_{TM}$  and  $F_{SM}$  are the molecular fluxes of heat and salinity respectively, and  $\kappa_T$  and  $\kappa_S$  are the molecular diffusivities of heat and salt, respectively.

Since  $\kappa_T \gg \kappa_S$ , for  $\alpha \Delta T$  and  $\beta \Delta S$  of the same order of magnitude, the density flux  $F_\rho = \rho \beta F_{SM} - \rho \alpha F_{TM} < 0$ . The rapid molecule diffusion of temperature, relative to salt, produces a downward density flux across the interface. The region immediately below (above) the interface becomes denser (lighter), which maintains the top-heavy convection in mixed layers. Figure 4 illustrates the physical mechanism for diffusive layering.

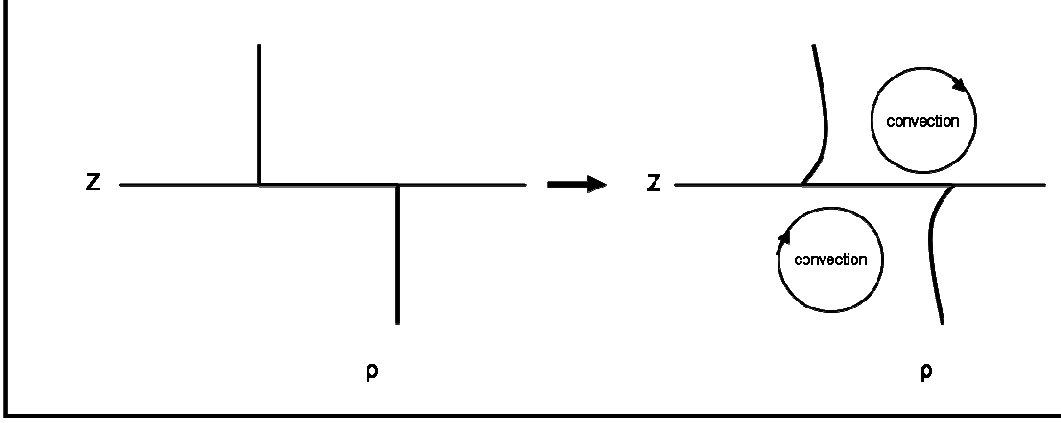


Figure 4. Physical mechanism behind diffusive layering.

There are several regions of the world's oceans with the potential for double-diffusive convection, including the Arctic Ocean (Kelley et al., 2003). The intensity of diffusive convection is controlled by the so-called density ratio, which, for the diffusive convection case, is defined as:

$$R_\rho = \frac{\beta \Delta S}{\alpha \Delta T} \quad (1)$$

where:

$$\begin{aligned} \alpha &= -\frac{1}{\rho} \left( \frac{\partial \rho}{\partial T^*} \right)_{S^*, P^*} \\ \beta &= \frac{1}{\rho} \left( \frac{\partial \rho}{\partial S^*} \right)_{T^*, P^*} \end{aligned} \quad (2)$$

Fluxes decrease with increasing density ratio. The range  $1 < R_\rho < 10$  is most susceptible to diffusive convection (Kelley et al., 2003). Analysis of Arctic density ratios

shows that the majority of the Arctic Ocean, specifically the Beaufort Gyre, has density ratios in the 3-10 range. (Figure 5)

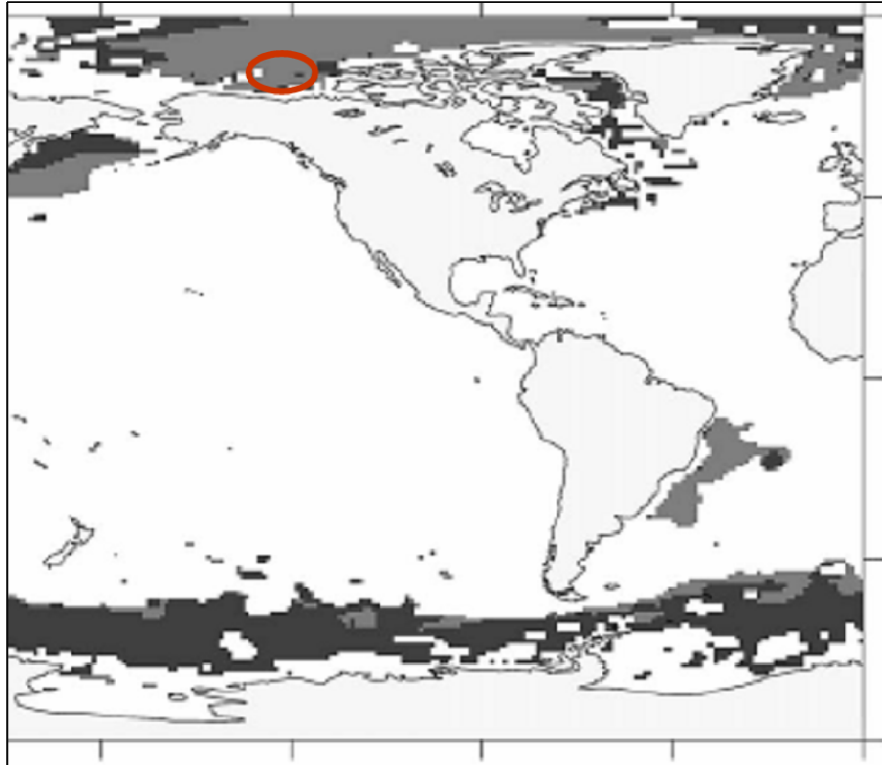


Figure 5. Regions susceptible to double diffusion. The light grey areas indicate where density ratio is from 3-10. Dark grey indicates  $1 \leq R_\rho < 3$ . The red circle indicates the Beaufort Gyre.

The Arctic is diffusively stratified due to the process of ice formation, brine rejection, and subsequent melting. The process creates the cold, fresh layer that lies on top of the warm, salty water carried from the Atlantic Ocean to the Arctic, through typical ocean circulation. Figure 6 illustrates Arctic currents and circulation patterns. Figure 7 provides a vertical cross section of the Arctic Ocean.



Figure 6. Arctic circulation pattern, resulting in conditions favorable for diffusive convection.  
(Illustration by Jack Cook, Woods Hole Oceanographic Institution.)

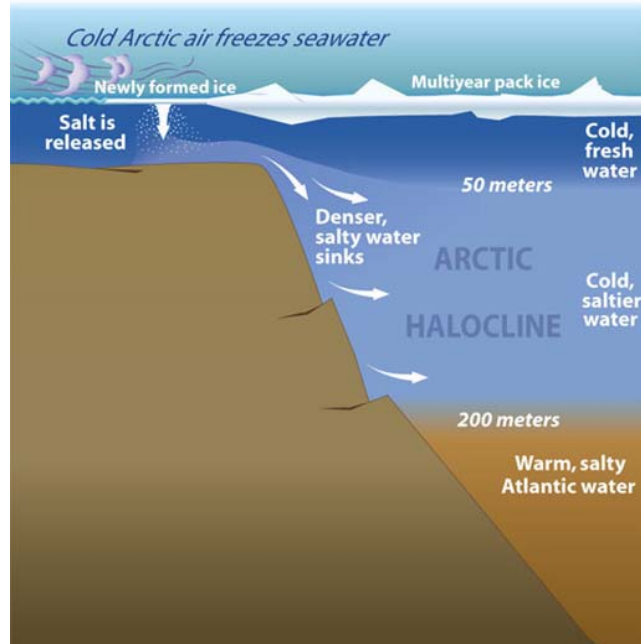


Figure 7. Cross section of Arctic water mass. Cold, fresh water overlies warm, salty Atlantic water.  
(Illustration by Jayne Doucette, Woods Hole Oceanographic Institute.)

In Figure 8 Fernando (1987) simulated the layering process by heating a salinity gradient from below. The diffusive layers are indicated in the diagram. Similar laboratory simulations have also been conducted using a sugar solution as the denser liquid. Figure 9 is a more completely evolved set of diffusive layers in the laboratory. Turner (1968) used this shadowgraph to show the scale of layers.

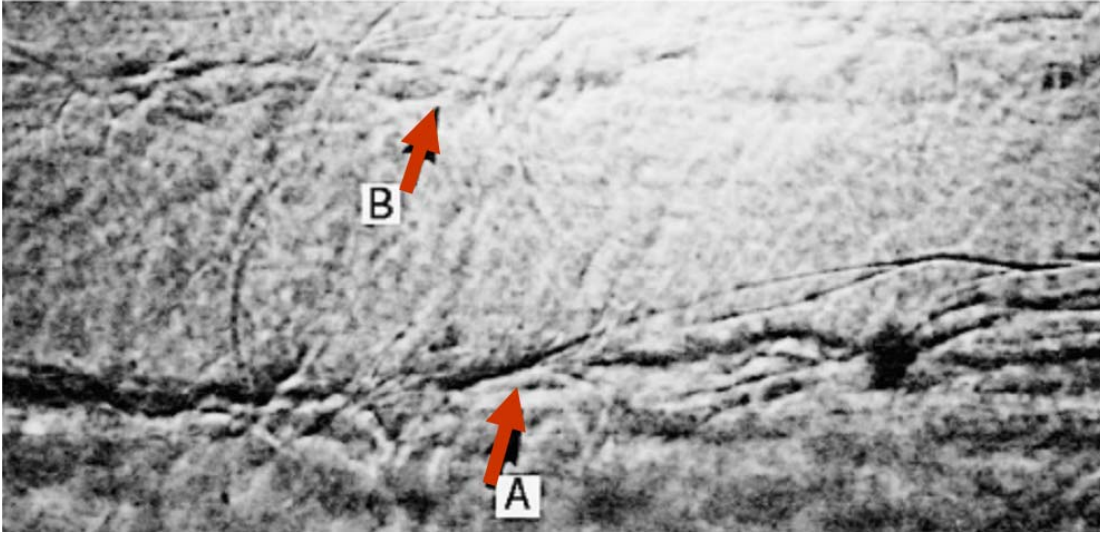


Figure 8. Side view of diffusive layering created by heating a salt gradient from below, after Figure 6 (Kelley 2003) A is the first quasi-stationary interface. B is the secondary interface, forming above it.

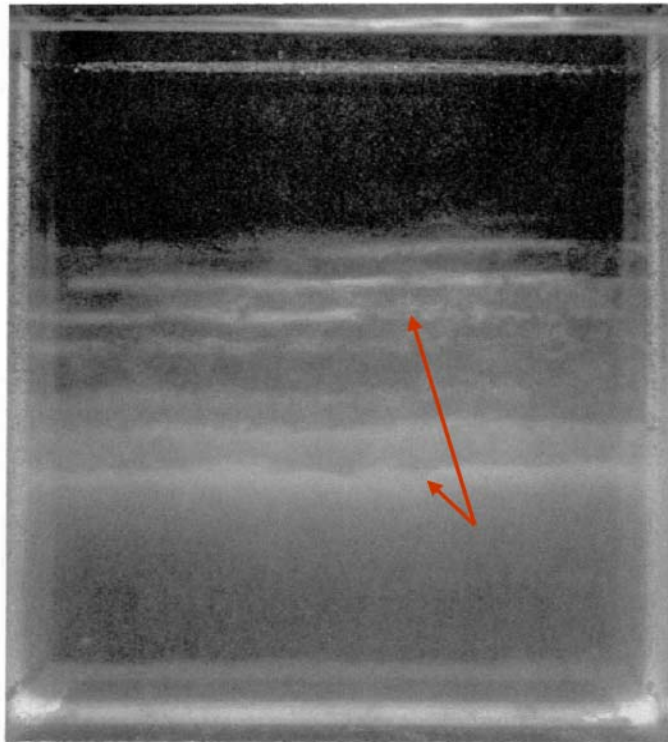


Figure 9. A series of convecting layers and heat-salt diffusive interfaces (Turner 1968).

## B. THEORETICAL BACKGROUND

Turner (1965) hypothesized that if steps are sufficiently large ( $H \rightarrow \infty$ ), the dependence of the vertical fluxes of temperature and salinity ( $F_T$  and  $F_S$ ) on  $H$  would be weak, and therefore fluxes would be determined by the temperature and salinity variations ( $\Delta T, \Delta S$ ) across the step:

$$\begin{aligned} F_T &= F_T(\alpha\Delta T, \beta\Delta S, \kappa_T, \kappa_S, \nu, g) = F_T(\alpha\Delta T, R_\rho, \kappa_T, g, \tau, P_r) \\ F_S &= F_S(\alpha\Delta T, \beta\Delta S, \kappa_T, \kappa_S, \nu, g) = F_T(\alpha\Delta T, R_\rho, \kappa_T, g, \tau, P_r) \end{aligned} \quad (3)$$

where  $\nu$  is viscosity,  $\tau$  is the diffusivity ratio and  $P_r$  is the Prandtl number  $\left(\frac{\nu}{\kappa_T}\right)$ .

Using the dimensional argument that a non-dimensional number can depend only on other non-dimensional numbers, Turner then suggested that the so-called Nusselt number,

$$Nu = \frac{F_T}{\kappa_T \frac{\Delta T}{H}}, \text{ measuring the fluxes would be related to the}$$

Raleigh number, measuring boundary forcing:  $R_a = \frac{g\alpha\Delta TH^3}{\kappa_T\nu}$ .

$$Nu = C(R_a)^n \Rightarrow \alpha F_T = \left(\frac{g\alpha\Delta TH^3}{\kappa_T\nu}\right)^n * \kappa_T \frac{\alpha\Delta T}{H} \quad (4)$$

From (3), we know that there should be no dependence on  $H$  in (4), therefore  $n=1/3$  or  $\alpha F_T \sim (\alpha\Delta T)^{\frac{4}{3}}$ . These equations are called the "4/3 Flux Laws". (Turner 1973)

Another non-dimensional quantity of interest is the flux ratio:  $\gamma = \frac{\beta F_s}{\alpha F_T}$ , which measures the fraction of the potential energy lost by temperature stratification that goes into the potential energy of salt stratification.

Turner (1965), argued, on the basis of dimensional considerations and laboratory experimentation, that for given molecular properties, the flux ratio is a function of  $R_\rho$ . Experiments yield a striking result that for  $R_\rho > 2$  the flux ratio remains constant to within the experimental error. In the laboratory this mean value is  $\frac{\beta F_s}{\alpha F_T} = 0.15$ , with maximum heat density flux for a given  $\Delta T$  occurring at  $R_\rho = 2$ . Figure 10 is a plot buoyancy flux ratio versus density ratio in the laboratory.

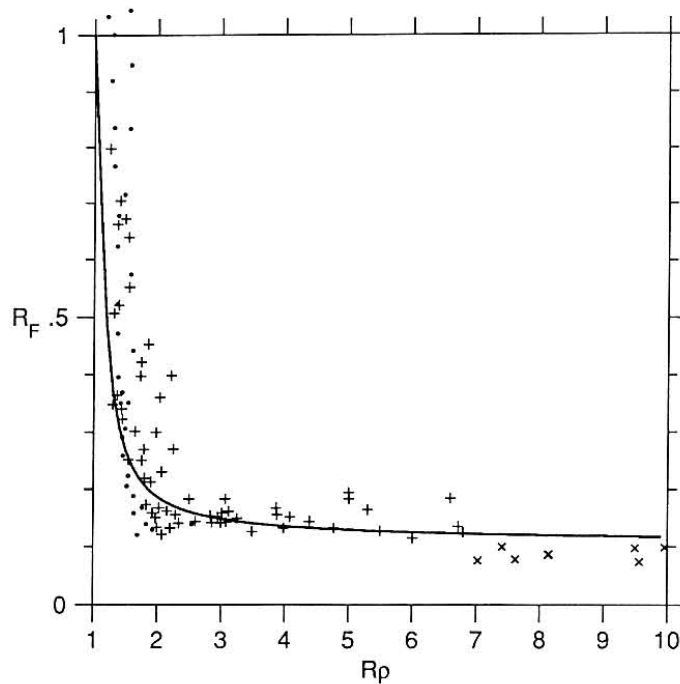


Figure 10. Buoyancy flux ratio  $R_F(R_\rho)$  for diffusive convection in the laboratory. Data from three different laboratory sources Crapper (1975), Turner (1965), and Newell (1984) from Kelley (1990). The solid line is the empirical fit.

The aforementioned models offer simple conceptual explanations for the dependences of vertical fluxes on temperature and salinity variations across the steps ( $\Delta T, \Delta S$ ). It follows that knowledge of what determines  $\Delta T$  in the staircases is necessary. Kelley (1988) and Radko (2005) suggest that a layer-merging process controls step characteristics. This merging process, which will be discussed further in Chapter III, can be defined as the coalescence of thin, adjacent layers to form new, thicker layers, and their eventual equilibration. The major goal of this study is to examine the validity of flux law models and predictions of merging theory. For that, we turn to Arctic data.

### **C. ICE-TETHERED PROFILER**

Originally, thermohaline staircases were not visible in ocean profiles. This was due to data taken only at standard levels versus a continuous profile of the region. In order to characterize the diffusive convective layers, high-resolution data are necessary. This study uses high resolution data collected from the Woods Hole Ice-Tethered Profiler Project.

In conjunction with the Beaufort Gyre Exploration Project, a team at Woods Hole Oceanographic Institute (WHOI) has launched several Ice-Tethered Profilers (ITP's) in the Beaufort Sea. Analysis of diffusive convection primarily uses data from ITP1 and ITP 3.

ITP's are moored profilers that are designed to make daily measurements of water, pressure, salinity (conductivity), and temperature in a region where ice impedes access and collection of this data. Designed to last for three years when deployed, as long as the ice floe survives, the profiler sends its measurements and GPS location to a surface float, which is then relayed back to WHOI. The profiler is made up of a small surface capsule, an 800 meter line, a moored profiler, and a small anchor. The profiler is modified so to fit through a 10" hole in the surface (Krishfield et al., 2006).

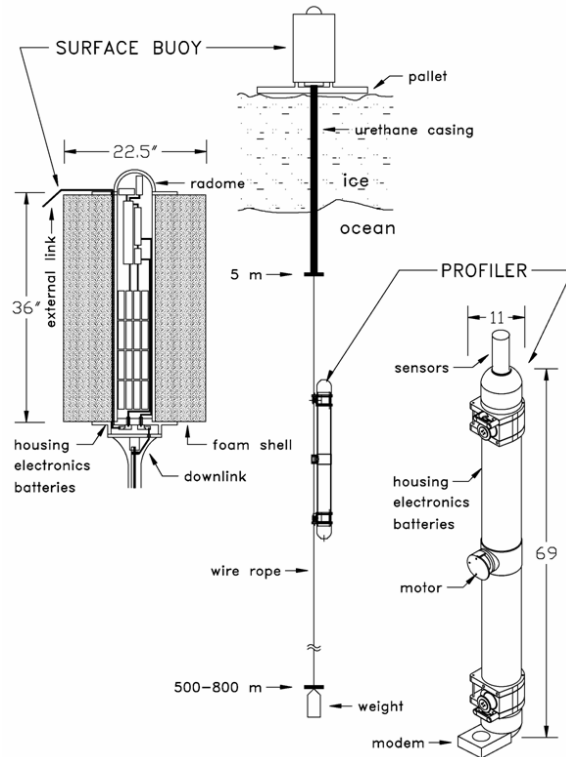


Figure 11. Schematic of Ice-Tethered Profiler (Krishfield et al., 2006).

The high resolution (25 centimeter) data posts to the WHOI ITP website for further analysis in its raw form. There are future plans to de-spike, filter, and correct the data using a sensor response correction (Johnson, 2007). These corrections should occur in the fall of 2007 and be considered for future work.

ITP 1 was the second of seven ITP's deployed. It was launched in the Beaufort Sea on August 15, 2005 at  $78^{\circ} 51.1$  N,  $150^{\circ} 15.9$  W during the JWACS 2005 cruise on the CCGS Louis S. St. Laurent. ITP1 was deployed on a 4.6 meter thick multiyear ice floe in a location designed to drift through the Beaufort Gyre Observing System (BGOS) array over the following year. ITP3, on August 23, 2005 at  $77^{\circ} 36.1$  N,  $142^{\circ} 11.8$  W, during the same cruise. It was deployed on a

3.5 meter thick multiyear ice floe in a location designed to drift through the Beaufort Gyre Freshwater Experiment (BGFE) array during the following year. Both units operate on a fast sample schedule of 4 one-way profiles between 10 and 760 meters depth each day.

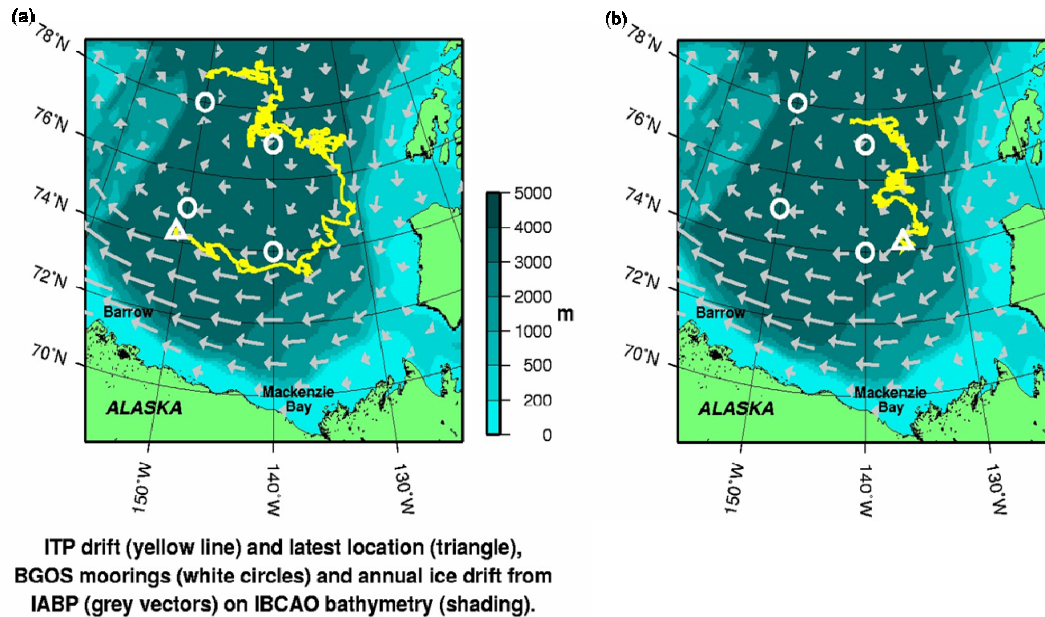


Figure 12. ITP 1 and ITP 3 drift tracks. (a) Drift track for ITP 1 and (b) is ITP3 drift track. From Woods Hole Oceanographic Institute Ice Tethered Profiler site (<http://www.whoi.edu/itp/data.html>).

THIS PAGE INTENTIONALLY LEFT BLANK

## II. CHARACTERISTICS OF THERMOHALINE STAIRCASES

### A. STEADY CHARACTERISTICS

The temperature, pressure, and conductivity raw data were used to create temperature-depth and salinity-depth profiles through the diffusive layer, characterized by prominent staircases. In the Beaufort Gyre Region, "staircase" structures were prominent from depths of about 200 to 400 meters. Therefore, all analyses were computed within that depth range. Figures 13 and 14 are temperature-depth and salinity-depth profiles illustrating the staircase characteristics. As denoted in Figure 13,  $H$  is defined as the distance between the midpoints of adjacent interfaces. Figure 14 indicates  $\Delta S$  measurements.  $\Delta T$  is found in the same manner. All vertical calculations were conducted with this data. The step is defined as the vertical rise between two adjacent interfaces.  $\alpha$  and  $\beta$  were calculated using the MATLAB seawater toolbox. Although they vary with depth, average values of  $\alpha$  are  $6 \times 10^{-5} \text{ K}^{-1}$  and  $\beta$  are  $8 \times 10^{-4} (\text{PSU})^{-1}$ . Average  $\Delta T$  was 0.04 degrees Celsius, and average  $\Delta S$  values were 0.01 PSU. The density ratios  $\left( R_\rho = \frac{\beta \Delta S}{\alpha \Delta T} \right)$ , computed for the ITP data, ranged from 3-7. Table 1 shows the data for ITP 1 and ITP 3 averaged by month.

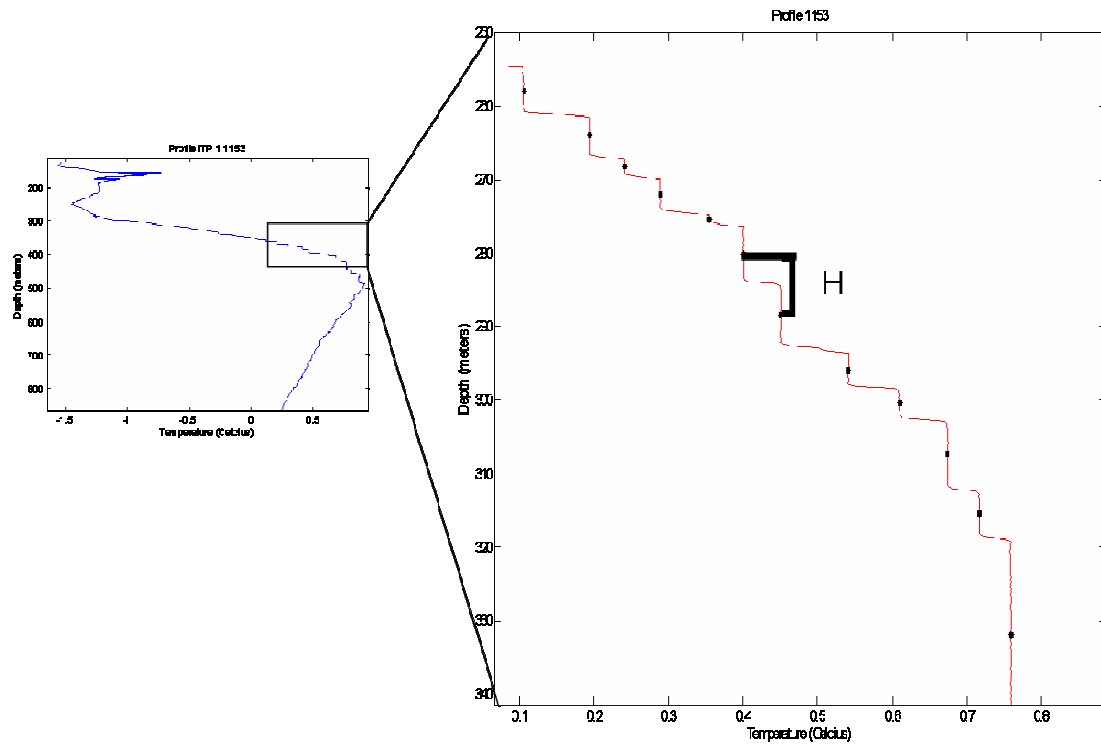


Figure 13. Temperature Depth Profile. The section of the profile is highlighted. H calculations are determined from the midpoint of each staircase depth.

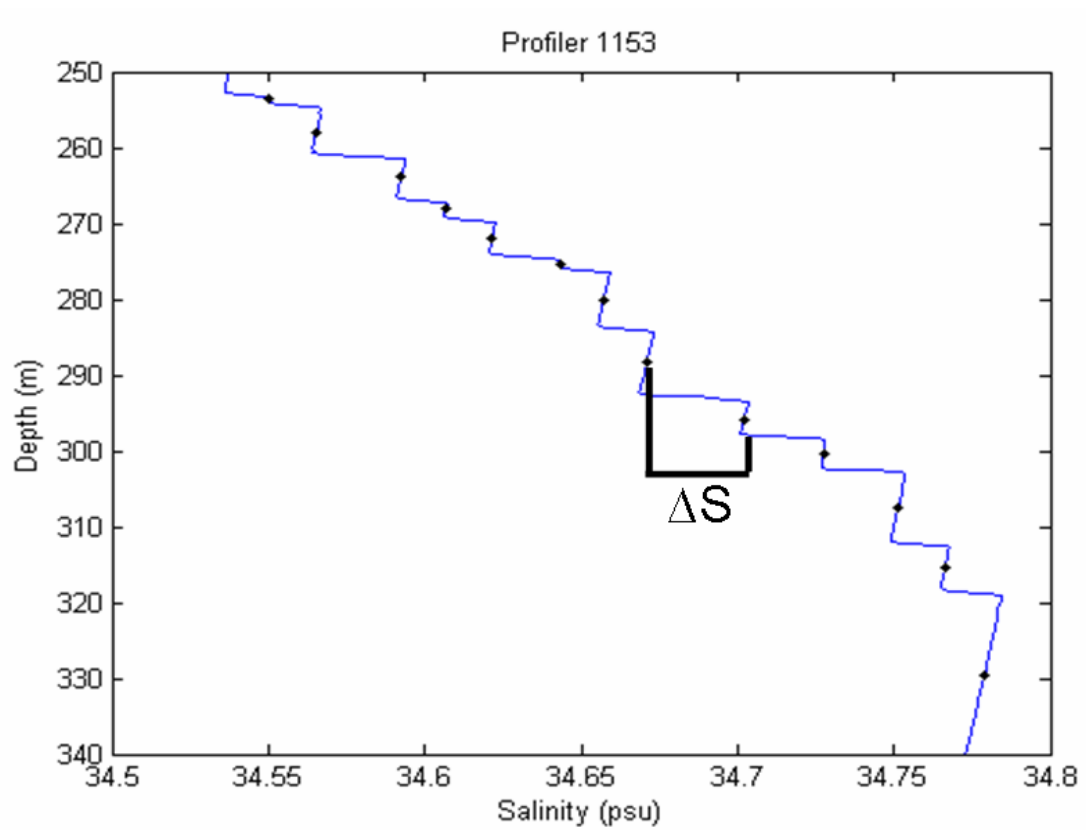


Figure 14. Salinity depth profile. Same location as previous figure. (Salinity is calculated using MATLAB polyfit to de-spike data).

		$\Delta T$	H(m)	Rp
ITP1				
September	2005	0.0403	4.1635	3.2713
October		0.0421	4.7896	3.6998
November		0.0437	4.6067	3.8795
December		0.0466	4.2825	4.759
January	2006	0.0437	4.1593	3.8973
February		0.0434	3.8276	3.8536
March		0.0456	4.3723	3.7838
April		0.0406	4.0872	3.8512
May		0.0397	3.4183	4.0875
June		0.0429	3.9029	4.1846
July		0.0472	4.31	4.3198
August		0.0441	3.9876	4.6595
September		0.0435	4.0714	4.9589
October		0.0466	4.2825	4.759
ITP3				
September	2005	0.0373	3.2653	5.5181
October		0.0432	3.6059	4.548
November		0.0394	3.5775	4.6802
December		0.0394	3.4346	4.8329
January	2006	0.0378	3.0995	4.7914
February		0.04115	3.3285	4.638
March		0.0455	3.8186	4.4491
April		0.046	3.5688	4.2637
May		0.0455	3.6922	4.3631
June		0.0477	4.1085	4.734
July		0.0356	2.7624	5.4397
August		0.0391	3.1684	5.3817
Average over both profilers		0.0426	3.8342	4.446

Table 1. Average data from ITP 1 and ITP 3 by month and over the entire data set.

Figure 15 plots  $\alpha\Delta T$  (non-dimensional temperature variation with depth) as a function of  $H$  (calculated step height.) Although only the month of January is presented, similar results were obtained for each month. From this comparison, it is theorized that the change in temperature is relatively linear, and is nearly independent of the height of the step. The slightly negative slope is caused by the dependence by  $\alpha$  on pressure. In general,  $H$  values increase from about 2 meters at a depth of 240 meters to above 20 meters at a depth of 400 meters, while  $\Delta T$  remains on average of 0.04 degrees C. This observation is consistent with Turner's suggestion that the vertical fluxes of heat and salt are independent of step height (Equation (3)). Indeed, if the vertical fluxes  $F_T$  and  $F_S$  are vertically homogeneous, then  $\Delta T, \Delta S = \text{constant}$ . Figure 16 shows a similar relationship between salinity and  $H$ .

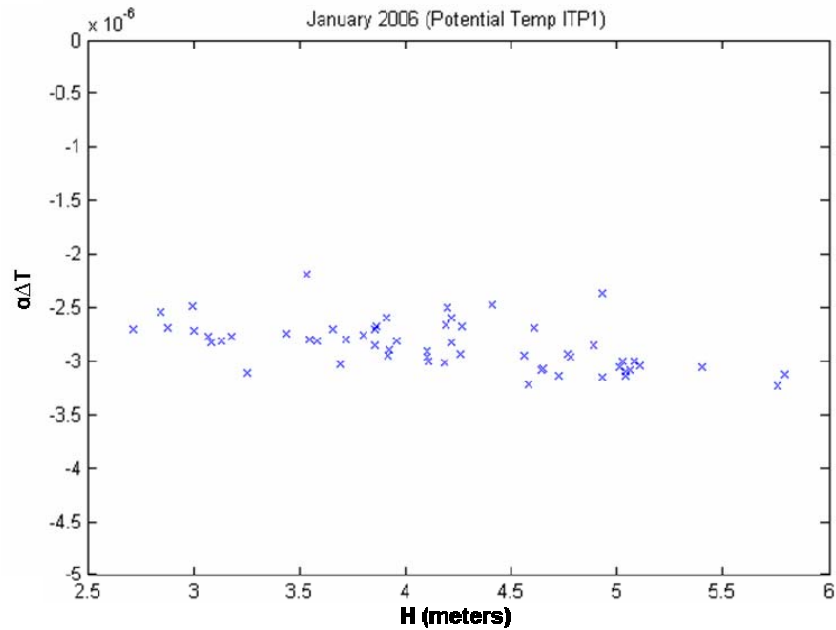


Figure 15. Non dimensional  $\alpha\Delta T$  is plotted as a function of layer thickness,  $H$  (meters).

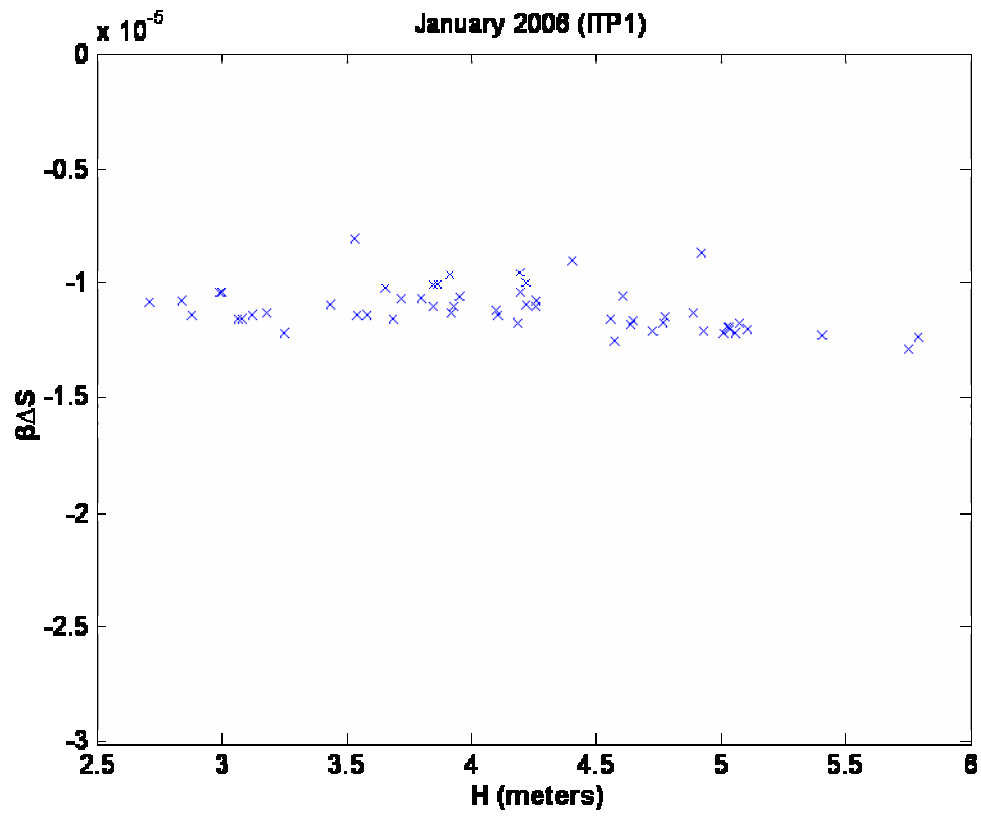


Figure 16. Non-dimensional  $\beta \Delta S$  is plotted as a function of layer thickness H (meters).

In Figures 17 and 18,  $\alpha\Delta T$  and  $\beta\Delta S$  are presented as a function of density ratio,  $R_\rho$ .

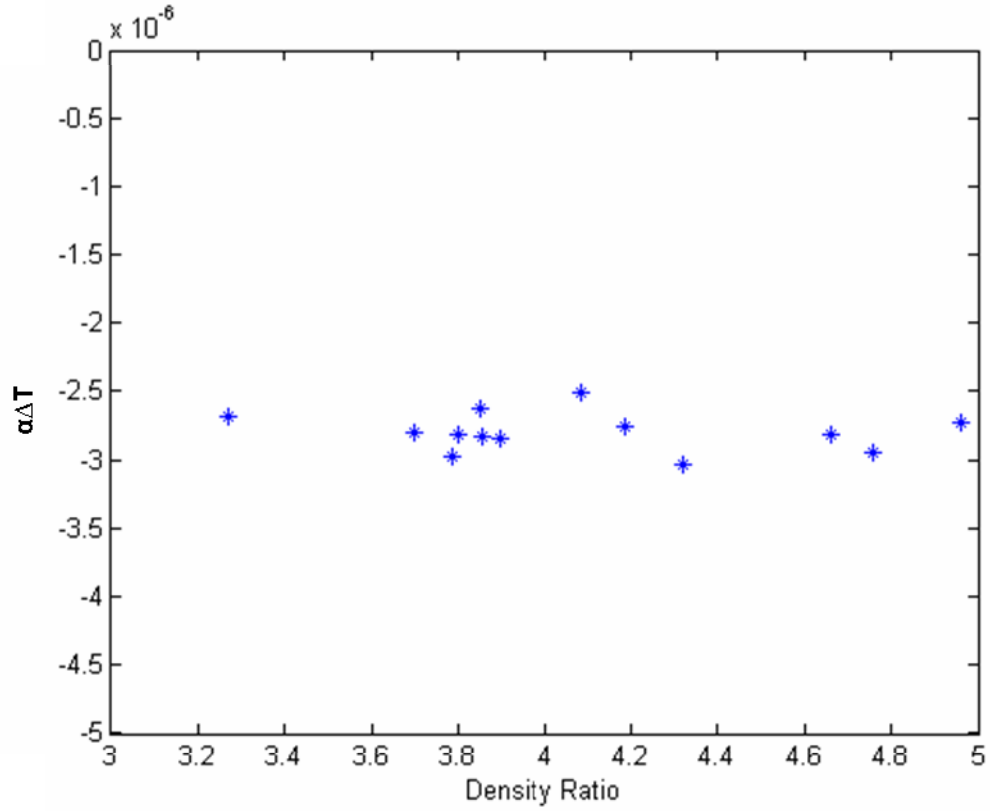


Figure 17. Comparison of  $\alpha\Delta T$  and  $R_\rho$  using average data from September 2005 to October 2006.

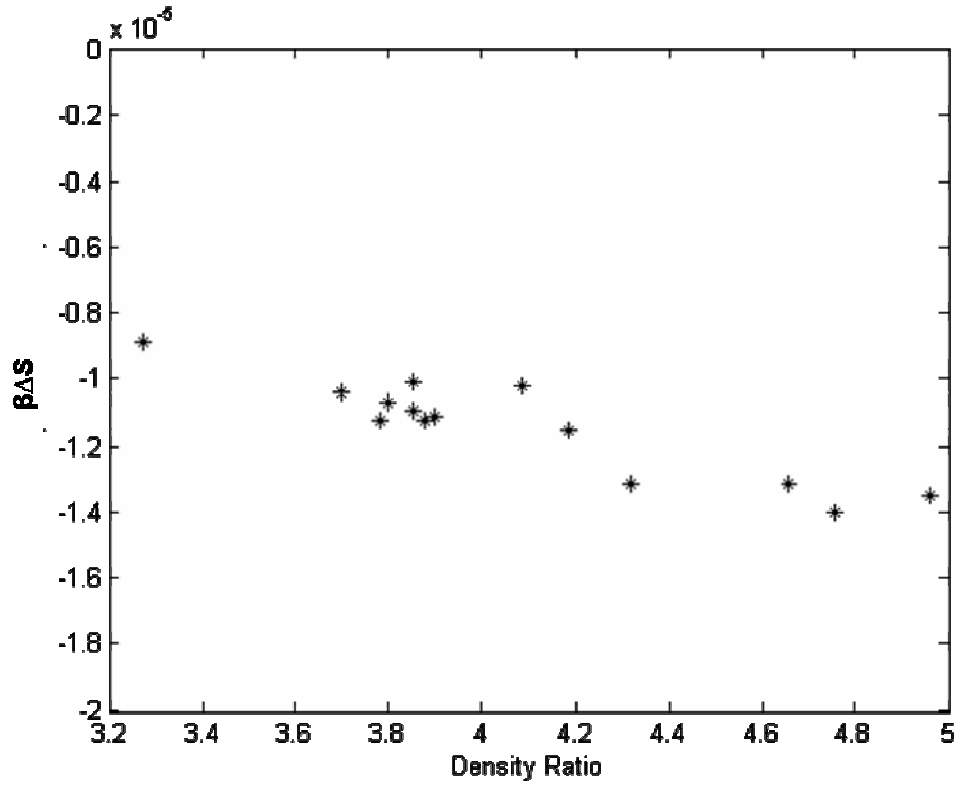


Figure 18. Comparison of  $\beta \Delta S$  and  $R_\rho$  using average data from September 2005 to October 2006.

In Figure 19, the density ratio over the interface is compared with the density ratio over the step. For this comparison, density ratio is first calculated over the step, and then calculated using two points on the adjacent interface. The density ratios for the interface and steps are then averaged by month and plotted. The increased value of  $R_{\rho_{Interface}}$  over  $R_{\rho_{Step}}$  is an indication of the ambiguity in the definition of density ratio, and leads to a possible source of error in the 4/3 flux laws.

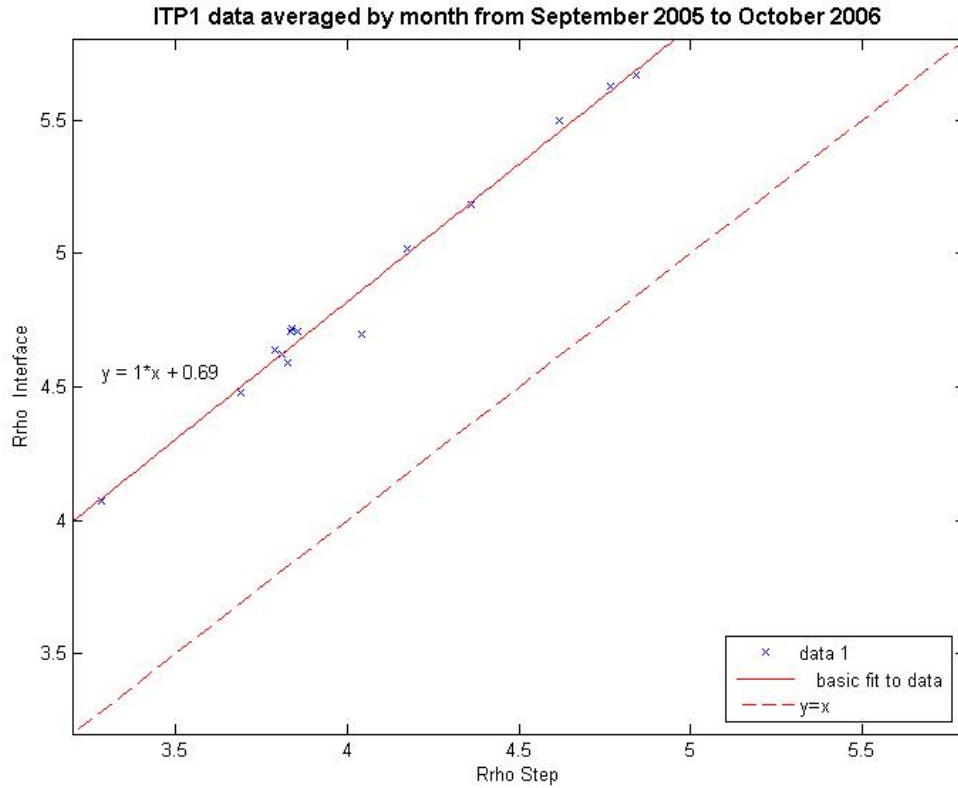


Figure 19. Comparison of density ratios over the interface and density ratios over the step.

There is general agreement in the literature that the double-diffusive temperature and salinity fluxes are controlled by the density ratio. While this relationship is known to exist, there is still considerable uncertainty in both the dynamics and values of fluxes in the thermohaline staircases using a straightforward extrapolation of the lab-based flux estimation. Padman and Dillon (1987) calculated thermohaline fluxes in the Beaufort Gyre to be about  $0.1 \text{ Wm}^{-2}$  for  $2 < R_\rho < 7$ . A comparison between the thermohaline staircases that Padman and Dillon explored and the current data indicate that in the 20 years between data collection,

there were significant changes in the water mass. This leads to changes in the calculated fluxes.

In 1987, the depth range of the staircases was 300-430 meters with  $\Delta T$  on order of 0.01 degrees C vice the 0.04 found today. There is a more fundamental difficulty with regards to the earlier estimates of fluxes in diffusive staircases. In addition to the differences in water column characteristics, Padman and Dillon's calculations were made using direct extrapolation from laboratory numbers. In the salt finger regime, such an extrapolation was long ago proven unreliable. In the diffusive convection regime, Kelley (1990) also suggested that direct application of the 4/3 Flux Law to ocean conditions is equally unreliable. In order to validate this theory, Radko (2007)'s merging theorem was applied to two components, temperature and salinity. These theoretical values, using laboratory results, were compared to the actual data. The result was confirmation that the 4/3 Flux laws cannot be directly extrapolated from the laboratory setup to diffusive convection in the ocean.

## B. EVOLUTIONARY PATTERN

Initially, the possibility of mergers existing in the ITP data came from a plot of conductivity versus time. Conductivity was used vice salinity because it could be taken in its raw form. In Figure 20, lines of constant conductivity, approximating the observations, are superimposed on the measured data. The merging events occurred twice in this figure – that is where the lines of constant conductivity meet and create fewer lines.

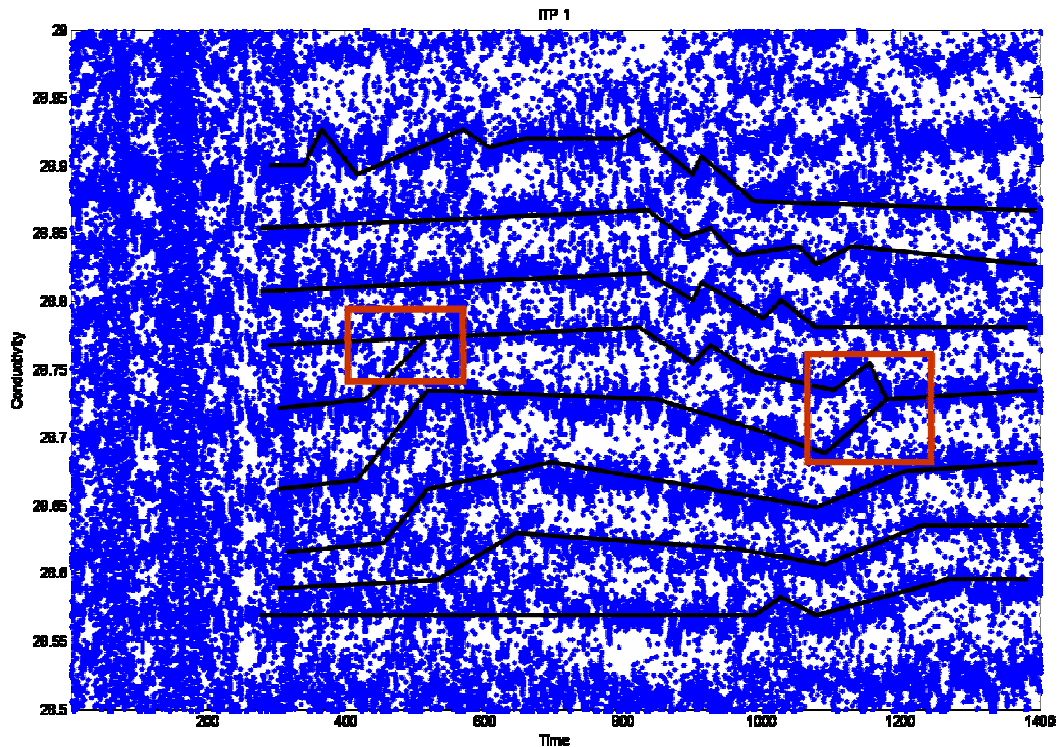


Figure 20. Examples of merging events, as seen from the inspection of the conductivity data.

Overall, we identified ten clear mergers to use in the following (Chapter III) theory-based analysis. Several of these mergers are presented in Figure 21. Visual inspection of all merging events suggest that layers merge when slightly stronger, in terms of temperature and salinity variations, interfaces grow, while weak interfaces decay and ultimately disappear. This is the evolutionary pattern classified by Radko (2007) as the B-merger scenario.

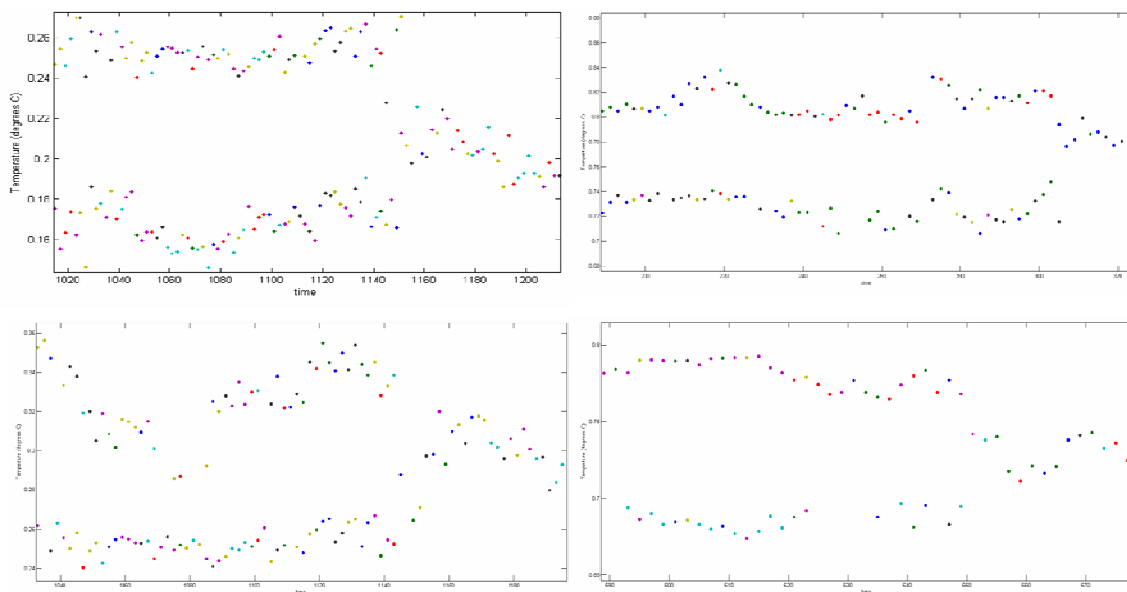


Figure 21. Temperature variation in time. Each data point represents temperature on a particular profile.

### III. MERGING THEOREM FOR A TWO COMPONENT FLUID

Radko (2007) theorized that the formation of diffusive layers starts with multiple, small-scale, homogenous density layers that merge until they reach equilibration. There are two types of merging processes. Radko defines them as H-merger and B-merger. The H-merger is defined when slightly thicker layers grow while thin layers shrink and ultimately disappear (Figure 22). In the case of B-merger (Figure 23), stronger interfaces grow at the expense of weaker interfaces. While theoretically both types are possible, data indicates that only the B-merger exists in the ocean, therefore the included derivations are limited to the B-merger.

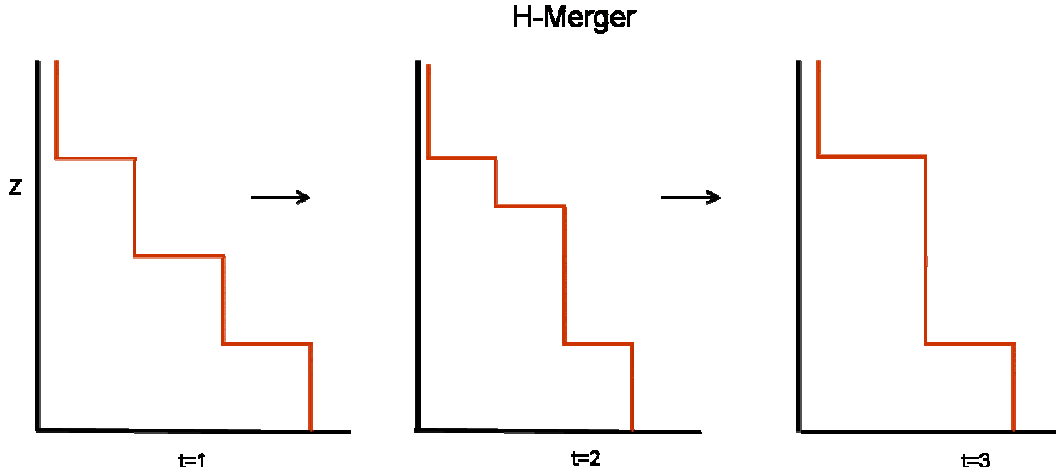


Figure 22. Schematic of H-merger evolution in time.

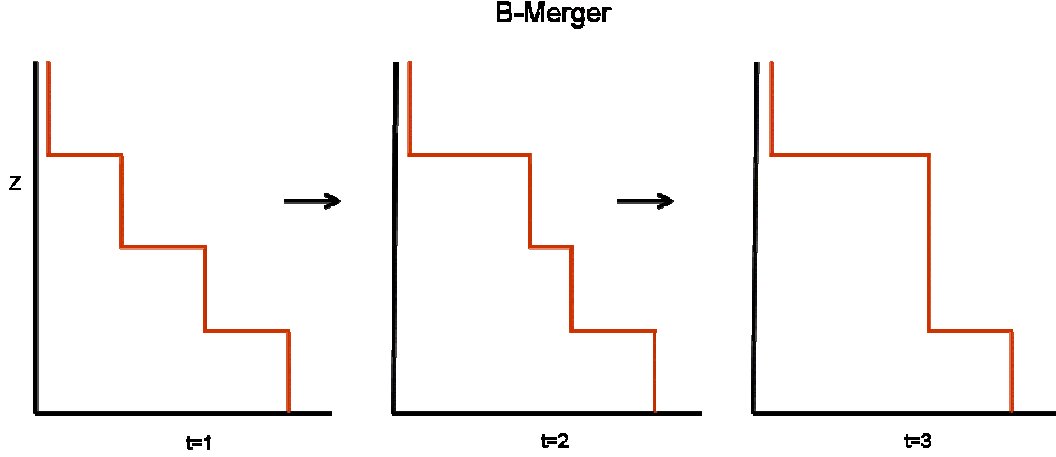


Figure 23. Schematic of B-merger evolution in time

The derivation for one component and one-dimensional mergers in Radko (2007) was modified to two components, salinity and temperature, yielding the following description of the B-merger events. This is accomplished by conducting a linear stability analysis for a series of identical steps and using it to formulate general criteria for B-merging events.

In order to establish the basic principals of the staircases evolution in time, we consider the stepped solution of the one-dimensional conservation equations:

$$\left. \begin{aligned} \frac{dT}{dt} &= \frac{dF^T}{dz} \\ \frac{dS}{dt} &= \frac{dF^S}{dz} \end{aligned} \right\} \quad (5)$$

The stepped solution is shown in Figure 24. Figure 24a represents a staircase consisting of identical steps, the basic steady-state. Figure 24b represents a slightly

perturbed state in which steps are no longer equal. The temperature-salinity variations across the two steps in Figure 24(b) are expressed as:

$$\left. \begin{aligned} T_{12} - T_{01} &= T - \delta \\ T_{23} - T_{12} &= T + \delta \\ S_{12} - S_{01} &= S - \varepsilon \\ S_{23} - S_{12} &= S + \varepsilon, \quad (\delta, \varepsilon) \ll (T, S) \end{aligned} \right\} \quad (6)$$

where  $T = (\partial \bar{T} / \partial z)H$  and  $S = (\partial \bar{S} / \partial z)H$  are the variations over one step in the undisturbed staircase in Figure 24(a) and  $(\delta, \varepsilon)$  are small perturbations. Assume that  $H$  is constant and equal where  $H$  is the distance between the interfaces at  $z = z_n$  and  $z = z_{n+1}$ .

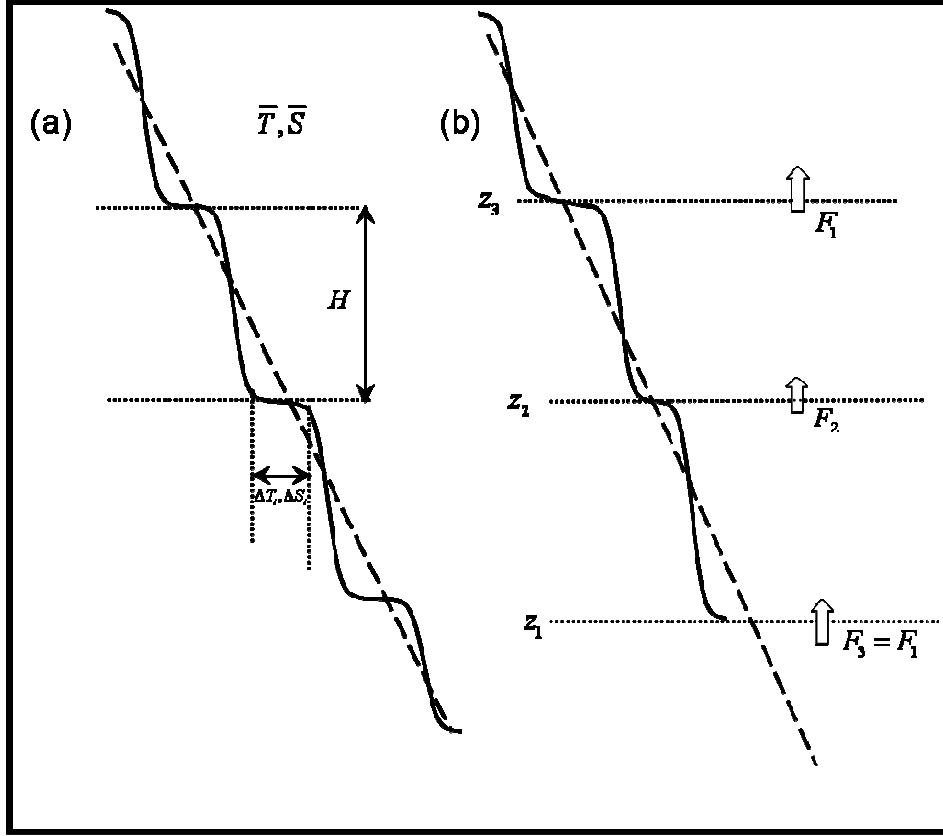


Figure 24. Schematic diagram illustrating the stability analysis for an infinite series of interfaces. (a) Basic state consisting of identical steps. (b) Perturbed state in which the  $T, S$  jumps at the even interfaces are slightly decreased, and the jumps at odd interfaces are increased.

Then integrating (5) over the interval  $[z_{\text{bot}}, z_{\text{top}}]$  where  $z_{\text{top}}$  and  $z_{\text{bot}}$  are two levels which do not vary in time:

$$\left. \begin{aligned} \int_{z_{\text{bot}}}^{z_{\text{top}}} \frac{\partial T}{\partial t} dz &= \int_{z_{\text{bot}}}^{z_{\text{top}}} \frac{\partial F^T}{\partial t} dz = F^T(z_{\text{top}}) - F^T(z_{\text{bot}}) \\ \int_{z_{\text{bot}}}^{z_{\text{top}}} \frac{\partial S}{\partial t} dz &= \int_{z_{\text{bot}}}^{z_{\text{top}}} \frac{\partial F^S}{\partial t} dz = F^S(z_{\text{top}}) - F^S(z_{\text{bot}}) \end{aligned} \right\} \quad (7)$$

Using the identity:

$$\left. \begin{aligned} \frac{d}{dt} \int_{z_{bot}}^{z_{top}} T dz &= \int_{z_{bot}}^{z_{top}} \frac{\partial T}{\partial t} dz \\ \frac{d}{dt} \int_{z_{bot}}^{z_{top}} S dz &= \int_{z_{bot}}^{z_{top}} \frac{\partial S}{\partial t} dz \end{aligned} \right\} \quad (8)$$

Equation (7) is rewritten as

$$\left. \begin{aligned} \frac{d}{dt} \int_{z_{bot}}^{z_{top}} T dz &= F^T(z_{top}) - F^T(z_{bot}) \\ \frac{d}{dt} \int_{z_{bot}}^{z_{top}} S dz &= F^S(z_{top}) - F^S(z_{bot}) \end{aligned} \right\} \quad (9)$$

Applying the integral relation in equation (9) to individual layers  $[z_n, z_{n+1}]$  yields, where  $F_i = F(z_i)$ :

$$\left. \begin{aligned} \frac{d}{dt} \int_{z_n}^{z_{n+1}} T dz &= F_n^T - F_{n+1}^T \\ \frac{d}{dt} \int_{z_n}^{z_{n+1}} S dz &= F_n^S - F_{n+1}^S \end{aligned} \right\}. \quad (10)$$

The major contribution to the integral of buoyancy in (10) comes from the interior part of layers where the buoyancy gradient is nearly uniform, and therefore,

$$\left. \begin{aligned} \int_{z_n}^{z_{n+1}} T dz &\approx T_{n+1} H \\ \int_{z_n}^{z_{n+1}} S dz &\approx S_{n+1} H \end{aligned} \right\} \quad (11) \quad \text{where } T_{n+1} \text{ and } S_{n+1} \text{ are the}$$

temperature and salinity values at the layer centers.

Applying (8) and (9) to two consecutive layers  $[z_n, z_{n+1}]$  where  $n=1, 2$  results in:

$$\left. \begin{aligned} \frac{d}{dt}(HT_{12}) &= F_2^T - F_1^T \\ \frac{d}{dt}(HT_{23}) &= F_3^T - F_2^T \\ \frac{d}{dt}(HS_{12}) &= F_2^S - F_1^S \\ \frac{d}{dt}(HS_{23}) &= F_3^S - F_2^S \end{aligned} \right\} \dots \quad (12)$$

Using equations (6) and (12), the equations for evolution of  $\delta$  and  $\varepsilon$  can be formulated, and then simplified using periodicity conditions.

$$\left. \begin{aligned} H \frac{d\delta}{dt} &= -2(F_2^T - F_1^T) \\ H \frac{d\varepsilon}{dt} &= -2(F_2^S - F_1^S) \end{aligned} \right\} . \quad (13)$$

Considering weak perturbations such that  $(\delta \ll T, \varepsilon \ll H)$  and linearizing (15) yields:

$$\left. \begin{aligned} \frac{d}{dt}\delta &= -\frac{2}{H}(F_2^T - F_1^T) \\ \frac{d}{dt}\varepsilon &= -\frac{2}{H}(F_2^S - F_1^S) \end{aligned} \right\} . \quad (14)$$

At this point, it becomes necessary to specify how the fluxes in (14) depend on temperature-salinity jumps across the steps. For that, we replace the instantaneous fluxes in interfaces  $F_n$  in (15) with the steady 'one-step' flux  $\tilde{F}$  (Radko 2007) based on the parameters of a region extending between the centers of two adjacent layers ( $z_{n-1n}$  and  $z_{nn-1}$ ):

$$\left. \begin{aligned} F_1^T &\approx \tilde{F}^T(T_{12}-T_{01}, S_{12}-S_{01}, z_{12}-z_{01}) \\ F_2^T &\approx \tilde{F}^T(T_{23}-T_{12}, S_{23}-S_{12}, z_{23}-z_{12}) \\ F_1^S &\approx \tilde{F}^S(T_{12}-T_{01}, S_{12}-S_{01}, z_{12}-z_{01}) \\ F_2^S &\approx \tilde{F}^S(T_{12}-T_{01}, S_{12}-S_{01}, z_{12}-z_{01}) \end{aligned} \right\} \quad (15)$$

The difference between fluxes at the adjacent interfaces in (14) reduces to:

$$\left. \begin{aligned} F_2^T - F_1^T &= 2\delta \frac{\partial \tilde{F}^T}{\partial \tilde{T}} + 2\varepsilon \frac{\partial \tilde{F}^T}{\partial \tilde{S}} \\ F_2^S - F_1^S &= 2\delta \frac{\partial \tilde{F}^S}{\partial \tilde{T}} + 2\varepsilon \frac{\partial \tilde{F}^S}{\partial \tilde{S}} \end{aligned} \right\}, \quad (16)$$

and (14) becomes:

$$\left. \begin{aligned} \frac{d}{dt}\delta &= -\frac{4\delta}{H} \frac{\partial \tilde{F}^T}{\partial \tilde{T}} - \frac{4\varepsilon}{H} \frac{\partial \tilde{F}^T}{\partial \tilde{S}} \\ \frac{d}{dt}\varepsilon &= -\frac{4\delta}{H} \frac{\partial \tilde{F}^S}{\partial \tilde{T}} - \frac{4\varepsilon}{H} \frac{\partial \tilde{F}^S}{\partial \tilde{S}} \end{aligned} \right\}. \quad (17)$$

Substitution of the normal modes  $(\delta, \varepsilon, h) = (\delta_0, \varepsilon_0, h_0) \exp(\lambda t)$  in (17) yields the eigenvalue equation for the B-growth rates:

$$\lambda_B^2 + \frac{4}{H} \left( \frac{\partial \tilde{F}^T}{\partial \tilde{T}} + \frac{\partial \tilde{F}^S}{\partial \tilde{S}} \right) \lambda_B + \frac{16}{H^2} \left( \frac{\partial \tilde{F}^T}{\partial \tilde{T}} \frac{\partial \tilde{F}^S}{\partial \tilde{S}} - \frac{\partial \tilde{F}^S}{\partial \tilde{T}} \frac{\partial \tilde{F}^T}{\partial \tilde{S}} \right) = 0 \quad (18)$$

If the free coefficient is small (to be expected since it is proportional to the flux ratio variation) the positive root can be further approximated by:

$$\lambda_B = \frac{4}{H} \frac{\frac{\partial \tilde{F}^S}{\partial \tilde{T}} \frac{\partial \tilde{F}^T}{\partial \tilde{S}} - \frac{\partial \tilde{F}^T}{\partial \tilde{T}} \frac{\partial \tilde{F}^S}{\partial \tilde{S}}}{\frac{\partial \tilde{F}^T}{\partial \tilde{T}} + \frac{\partial \tilde{F}^S}{\partial \tilde{S}}} \quad (19)$$

The tildes denote the equilibrium one-step parameters. The latter affords an attractive opportunity to validate the merging theory (Huppert, 1971; Kelley, 1988; Radko, 2005) by comparing the growth rates of the observed merging events with the theoretical prediction for  $F(R_\rho)$ .

#### IV. APPLICATIONS OF THE MERGING THEOREM TO OCEANIC DATA

In order to apply the merging theorem (19) to actual field data, explicit expressions for fluxes are needed. While little is known about the flux laws in the ocean, we assume that the general structure of the laboratory-derived flux laws pertain to the ocean, but additional calibration of amplitude is necessary. Adopting the derived flux laws, but recalibrating them for oceanic conditions, (e.g. Kelley 1990) yields:

$$\left. \begin{aligned} \alpha \tilde{F}^T &= AC \left( \frac{g k_T^2}{\nu} \right)^{1/3} (\alpha \Delta T)^{4/3}; \quad C = 0.0032 \exp(4.8/R_\rho^{0.72}) \\ \beta \tilde{F}^S &= \alpha \tilde{F}^T \gamma; \quad \gamma = \frac{R_\rho + 1.4(R_\rho - 1)^{3/2}}{1 + 14(R_\rho - 1)^{3/2}} \end{aligned} \right\} \quad (20)$$

"A" is an adjustable coefficient included to recalibrate Kelley-Turner flux laws for the ocean.

An alternative lab-based formulation was suggested by Marmorino and Caldwell (1976):

$$H_{SP} = (0.085) k_T \left( \frac{g \alpha}{\kappa \nu} \right)^{1/3} \Delta T^{4/3} \quad (21)$$

$$\frac{H}{H_{SP}} = 0.101 \exp \left\{ 4.6 \exp \left[ -0.54 (R_\rho - 1) \right] \right\} \quad (22)$$

Finally, substitute (20) and (22) into (19) and obtain specific solutions. Simplifying (19) takes the form:

$$\lambda_B = \frac{(\alpha \Delta T)^{\frac{1}{3}}}{H} F(R_\rho) \quad (23)$$

Now, we apply the ITP data. The exponential variation of  $\Delta T, \Delta S$  across the merging layers confirms the interpretation of the merging as an instability process. The growth rate of each merger is determined from the best fit of the exponent  $\exp(\lambda t)$  to  $(\Delta T_A - \Delta T_{A0})$ , where  $\Delta T_A$ , is the temperature variation in the merging layer, and  $\Delta T_{A0}$  is its value at the beginning of the merging event. Two examples of growth rate determination are provided. In the first example, the density ratio is slightly higher, leading to a smaller growth rate and a longer period for merging (Figure 25). In the second example, the density ratio is only slightly smaller, but the growth rate is twice as large, yielding a much shorter merging period (Figure 26).

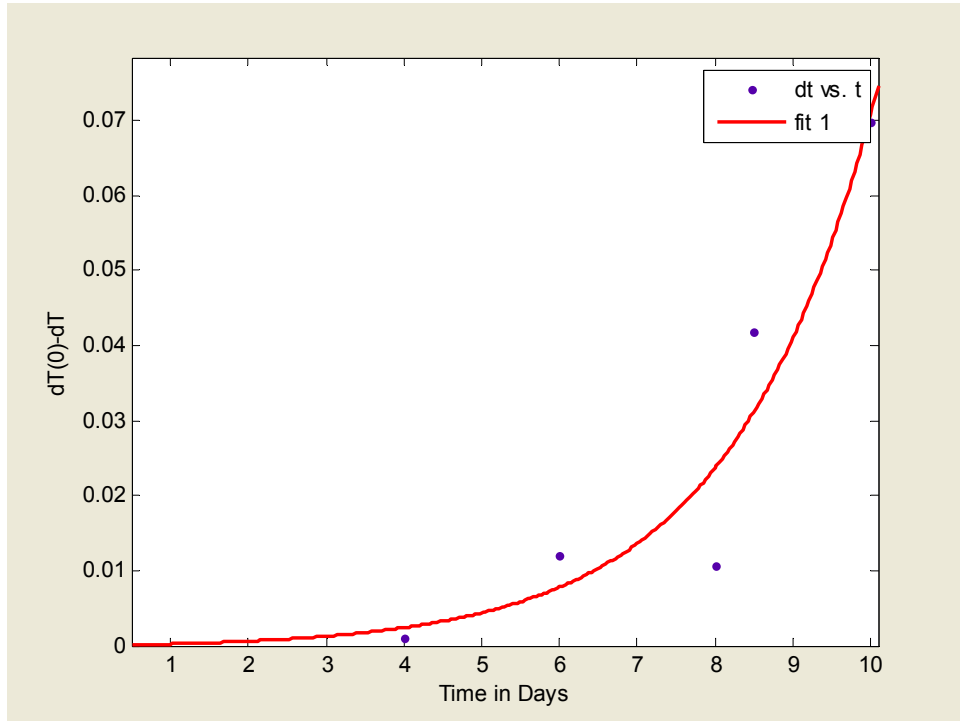


Figure 25. Change in temperature vs. time during the merging period. The normalized growth rate for this merger is  $4.7\text{E-}04$  and the density ratio is 2.8631.

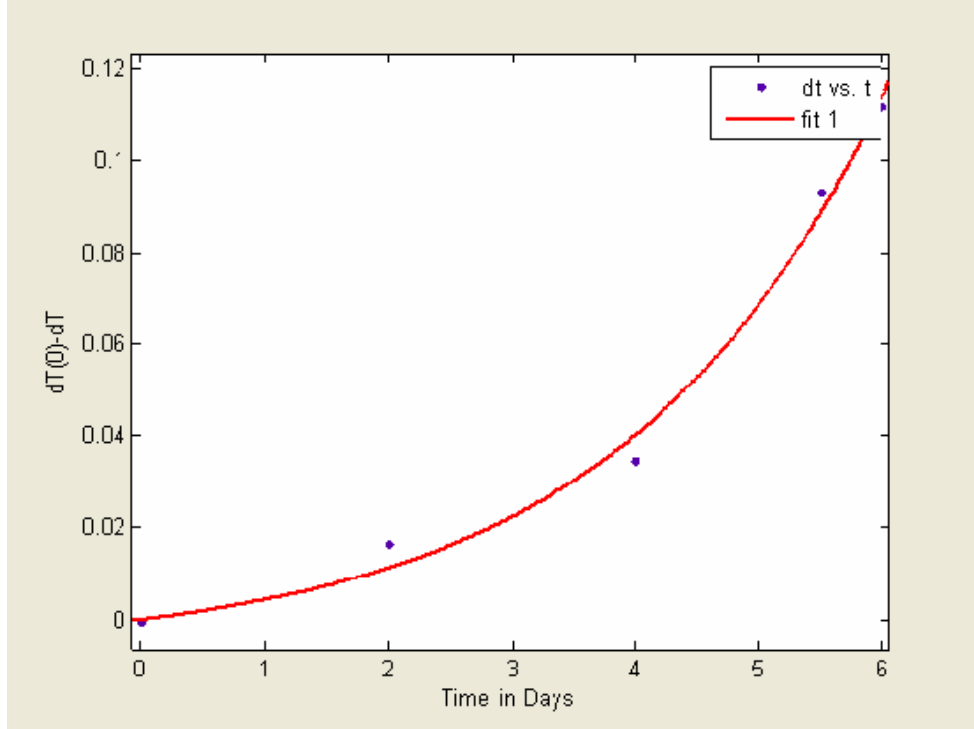


Figure 26. Change in temperature vs. during the merging period. The normalized growth rate for this merger is  $8.6E-04$  and the density ratio is 2.4035.

The merging growth rates are then normalized as follows:

$$\lambda_{normal} = \frac{\lambda H}{(\alpha \Delta T)^{1/3}} \quad (24)$$

where  $H$  is the initial step height and  $\alpha = 6e-5 K^{-1}$ . They are then compared with the normalized growth rates from the theoretical/laboratory values. Kelley (1990) suggested that the coefficient  $C$  in the  $4/3$  flux law differed based on density ratio. Based on laboratory estimates,

$$C = .0032 \exp\left(\frac{4.8}{R_{\rho}^{0.72}}\right) \quad (25)$$

This differs from Marmorino and Caldwell (1976) who suggested

$$C = 0.085 * 0.101 * \exp\left(4.6 \exp\left[(-0.54 \{R_{\rho} - 1\})\right]\right). \quad (26)$$

The differences in the calculations of laboratory data lead to questions regarding the precision of laboratory measurements. In order to estimate the error of the model predictions, both Kelley and Marmorino and Caldwell's formulations were independently used. Figure 27 is based on Kelley's expression, which required a coefficient  $A=30.008$  to fit Beaufort Gyre data. Marmorino and Caldwell's coefficient, was  $A=15.75$  and the corresponding prediction for  $\lambda_{norm}$  is shown in Figure 28. Table 2 shows a numerical comparison of the fit.

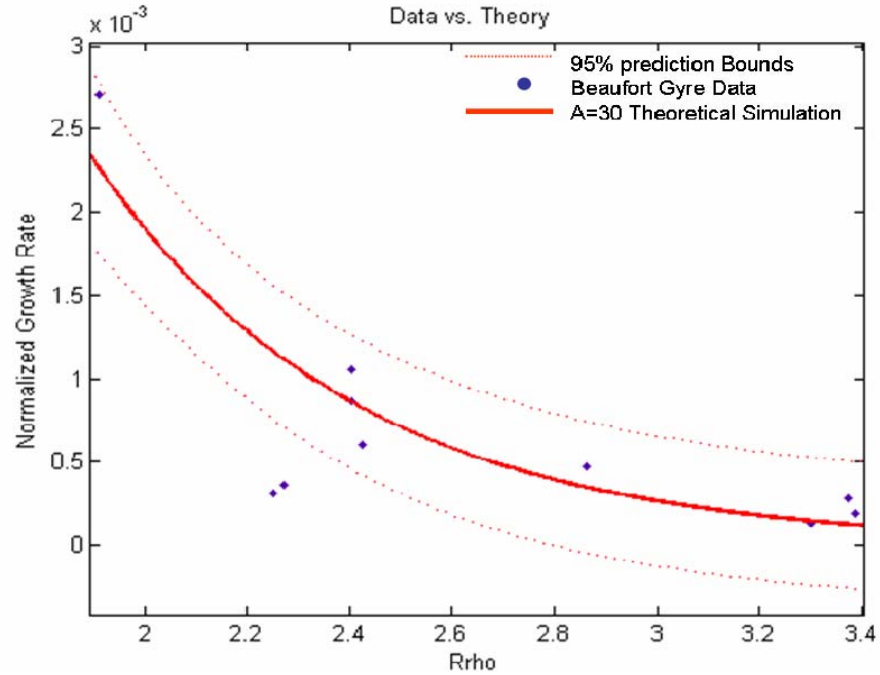


Figure 27. Using the coefficient  $A=30$ , theoretical data fits Beaufort Gyre data within 95% prediction bounds.

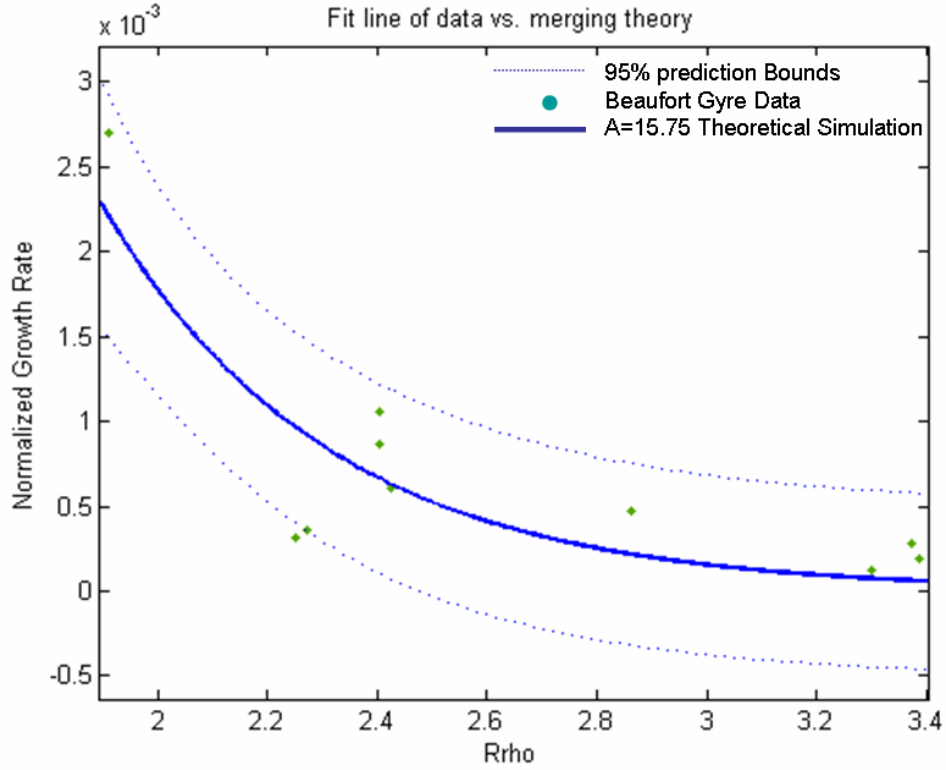


Figure 28. Using the coefficient  $A=15.75$  applied to Marmorino and Caldwell (1976), theoretical data fits Beaufort Gyre data within 95% prediction bounds.

$R\rho$	$\Delta T$	H	$\lambda$ normalized	$\lambda$ normalized A=30	$\lambda$ normalized A=15.75
1.9106	0.1572	24	2.70E-03	2.58E-03	2.48E-03
2.2509	0.1007	7	3.11E-04	3.11E-04	7.93E-04
2.2737	0.087	3	3.60E-04	3.60E-04	7.43E-04
2.4031	9.61E-02	4.6	1.06E-03	7.17E-04	5.24E-04
2.4035	1.12E-01	3	8.63E-04	7.17E-04	5.23E-04
2.4267	1.18E-01	5	6.08E-04	6.83E-04	4.93E-04
2.8631	6.99E-02	4	4.71E-04	3.16E-04	1.90E-04
3.2997	8.20E-02	3.7	1.28E-04	1.75E-04	9.25E-05
3.3728	7.91E-02	2.8	2.81E-04	1.60E-04	8.35E-05
3.3879	9.09E-02	3	1.90E-04	1.58E-04	8.18E-05

Table 2. Data comparison of calculated normalized growth rate from actual data and the normalized growth rates using a constant factor with the 4/3 flux law.

The coefficient  $A$ , which we believe is necessary to convert from laboratory simulations to ocean data leads to relatively high heat fluxes ( $H_F$ ) for low density ratios ( $1.9 < R_\rho < 3.4$ ). When applying the  $A$ -coefficient to characteristics of multiple thermohaline staircases, the average flux is  $6.65 \text{ Wm}^{-2}$  for Kelley's formulation and  $3.717 \text{ Wm}^{-2}$  for Marmorino and Caldwell's. The range of fluxes is obtained using ITP 1 data from April of 2006. Average  $\Delta T$ ,  $R_\rho$ , and  $H$  values were calculated in 20 meter increments from 220 to 360 meters (except for 320-360 meters where steps were too large to make accurate calculations from a 20 meter interval). This range covers 1211 steps. Table 3 shows the data averaged by layer.

Depth in meters	220-240	240-260	260-280	280-300	300-320	320-360
$\Delta T$	0.0426	0.0405	0.0423	0.0635	0.0439	0.0368
$\Delta S$	0.0132	0.0125	0.0118	0.0202	0.0145	0.0138
$R_\rho$	6.1626	5.5163	4.6419	4.9691	4.9435	5.6985
$H$ (meters)	2.3520	2.6326	3.1538	4.4798	6.0994	5.9379
Total Steps	317	306	275	157	70	86
Kelley's Flux Law						
HF w/A=1	0.1570	0.1637	0.2134	0.3327	0.2045	0.0126
HF w/A=19.6078	3.0783	3.2091	4.1853	6.5227	4.0099	0.2472
HF w/A=30	4.7090	4.9099	6.2648	9.9797	6.1351	4.1831
HF w/A=31.01522	4.8692	5.0761	6.6201	10.3175	6.3427	0.3910
Marmorino and Caldwell's Flux Law						
HF w/ A=1	0.1524	0.1606	0.2176	0.3370	0.2076	0.1366
HF w/ A=8.75	1.3333	1.4056	1.9039	2.9488	1.8162	1.1953
HF A=15.75	2.4000	2.5300	3.4270	5.3079	3.2691	2.1515
HF w/ A=17.955	2.7360	2.8842	3.9068	6.0510	3.7268	2.4527

Table 3. ITP 1 data for April 2006 in 20-40 meter layer increments.

Table 4 uses the averaged data from Table 1 to provide a range of possible heat fluxes in the Arctic. The range varies significantly based on the size of the coefficient A. This suggests that further study is necessary to determine the validity of the 4/3 flux law when applying it to ocean conditions.

Averages from Table 1		Original HF Wm <sup>-2</sup>	Range of A HF Wm <sup>-2</sup>	Low Bound HF Wm <sup>-2</sup>	Best Fit HF Wm <sup>-2</sup>	High Bound HF Wm <sup>-2</sup>
$\Delta T$ 0.0426	Marmorino	0.2360	8.75<A<17.96	2.0652	3.7174	4.2378
H(m) 3.8342	Kelley	0.2216	19.61<A<45.90	4.3459	6.6492	10.173255
Rp 4.446						

Table 4. Heat Fluxes in the Beaufort Gyre using the calibrated flux laws.

THIS PAGE INTENTIONALLY LEFT BLANK

## **V. ACOUSTIC APPLICATIONS**

### **A. EFFECTS OF THERMOHALINE STEPS ON ACOUSTIC TRANSMISSION**

The "fine-structure" and "microstructure" characteristics of diffusive convection described above were rarely considered to have an impact on acoustic transmission. However, with recent high-resolution ocean data illustrating the depth and range that thermohaline staircases cover, these small-scaled phenomena are given new consideration. Chin-Bing et al. (1994) studied the effects of the thermohaline staircase step-structure on ocean sound velocity profiles (SVP's) and then performed acoustic propagation simulations using the oceanographic data.

The simulations done by Chin-Bing et al., used data collected from the northeast coast of South America in the fall (October-November) of 1985. The staircases studied were the result of salt-fingers and therefore had different characteristics (i.e., step size and density gradients) from the present studies of thermohaline staircases. However, these results led to the initial consideration of acoustic propagation through diffusive convective layers.

### **B. INITIAL APPLICATION TO DIFFUSIVE CONVECTION**

Wide-angle capable, research-level, Parabolic Equation (PE) models were used to simulate long-range transmission loss through ocean thermohaline steps. The wide-angle models were used due to the deep ocean waveguide which supports fully retracted propagation for angles of  $\pm 15^\circ$ . Due to the sensitivity of PE models to range step and depth step, the

model was run decreasing range and depth steps until the results converged on a stable answer. This led to the use of range and depth step sizes of 1/24 the wavelength. The frequency choice of 50Hz gave an acoustic wavelength on the same order as the step-size in the SVP. The source depth was 400 meters, placing it in the mid-depth of the steps. Results were plotted for receiver depths of 200, 400, and 800 meters, that is, above, in, and below the step region respectively. In order to determine the importance of transmission loss through the staircases, a comparison was made between the transmission loss of the high-resolution step sound velocity profiles (SVP) and lower resolution data only taken at standard depths.

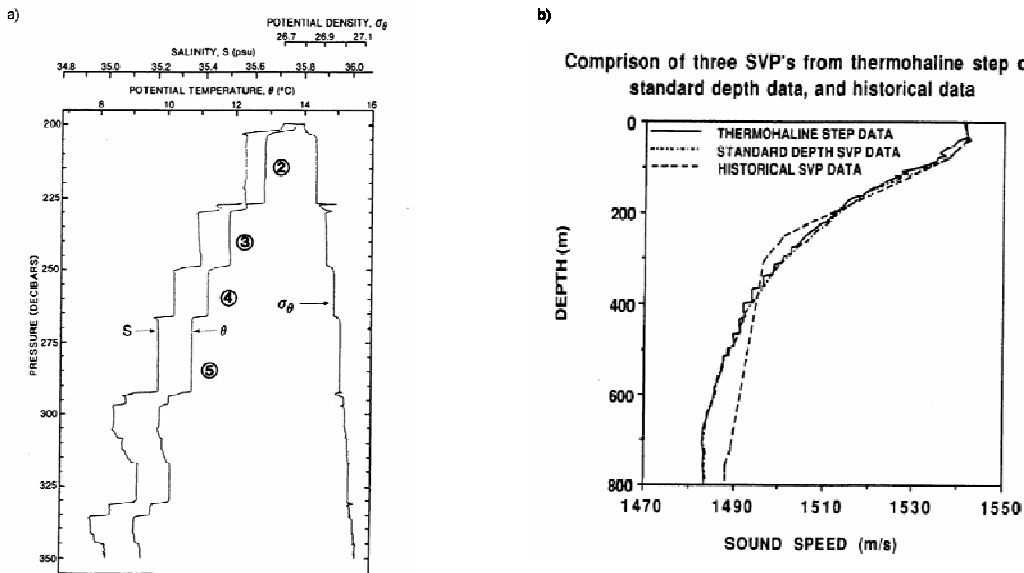


Figure 29. a) Typical temperature and salinity plot for salt finger region. Salinity, Potential Temperature and Density plots show thermohaline step characteristics. b) Sound velocity profiles showing the step data, standard depth profiles and historical averaged sound velocity profile data. From Chin-Bing et al. (1994).

The resulting simulation showed that when the receiver was above the step region there was very little difference when comparing the transmission loss of the two SVP data sets. The same determination was made when the receiver was under the staircase structure. There was, however, a significant difference within the step region--5 decibels over a 10-kilometer range. The greatest impact on the ray paths were when both the source and receiver were at 400 meters, both were within the staircase structure.

The numerical experiment then went on to test the effects of the staircases on backscatter. Using the same 50Hz source, a source depth of 100 meters below the surface was chosen. Chin-Bing et al. found that in the low frequency regime of the study, the staircases tend to have a negligible effect; however, they felt as the frequency of the acoustic field increased so should the magnitude of the backscatter. They surmise that given frequencies in the sonar range i.e. 3.0 kHz, the backscatter from thermohaline steps could be significantly important.

### **C. THE ARCTIC CASE**

From the above research, we thought it prudent to test the impact of the diffusive convection form of thermohaline staircases, given the probability of increased interest in the Arctic. The raw data from ITP profile 1013, chosen for its well formed staircase structure, was used for basic experimentation (Figure 30).

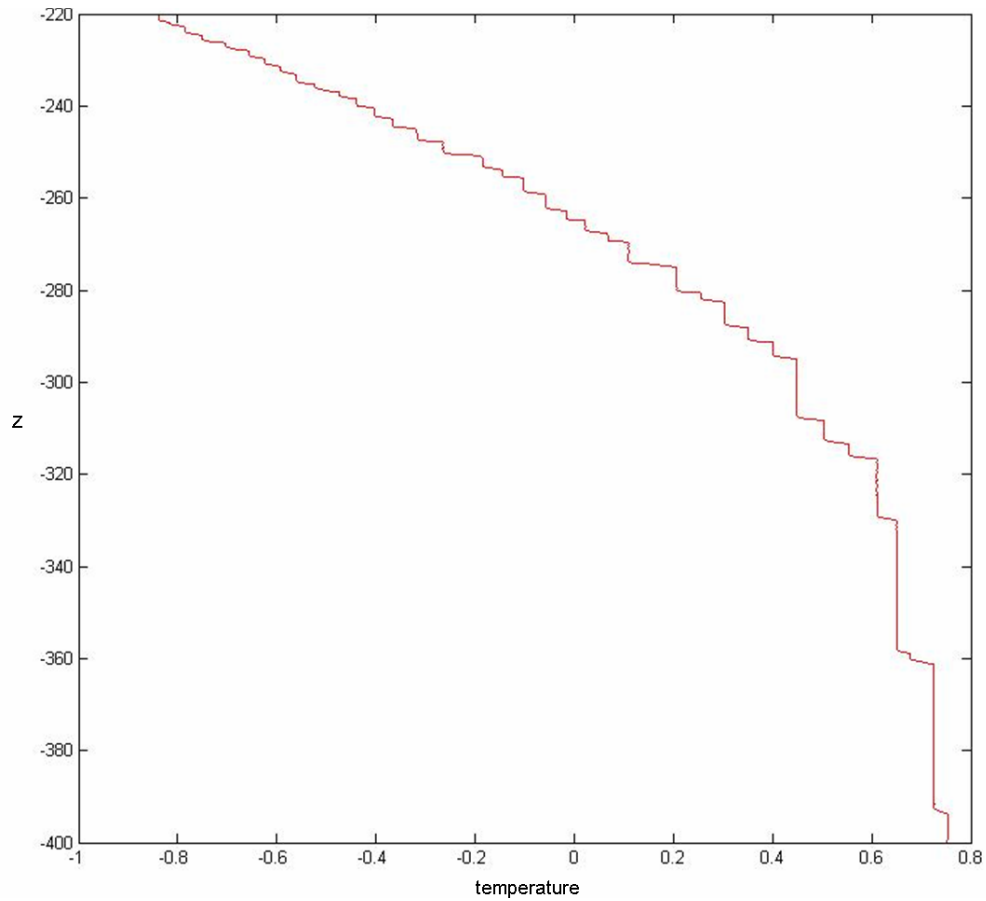


Figure 30. Temperature and depth profile used for acoustic simulation.

Raw temperature data and converted salinity (from conductivity) data was used for the idealized experiment. Using a basic fit of the data, the staircase structure was smoothed from the profile in order to offer a comparison in the effects of the microstructure on sound propagation. Using Del Grosso's Equation (Del Grosso 1974), sound speed profiles were calculated for simulation purposes. Figure 31 shows the two sound velocity profiles. The only region of the profiles that was smoothed was the staircase region, so that effects of other factors were not included in the calculated impact.

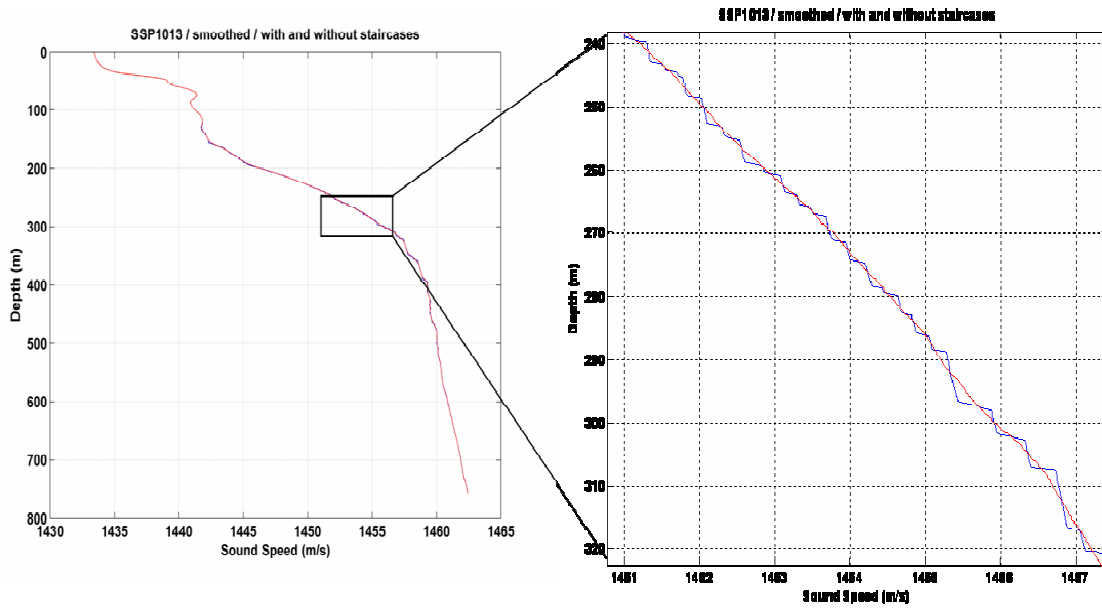


Figure 31. Sound Velocity Profile from ITP 1 raw1013 data. Red profile smoothes staircase structure, blue includes staircases. The graphic on the right is an enhancement to the SVP so that the staircase region is more visible.

The parameters for the simulation were a planar, perfectly reflecting surface. (This is not the case for under the ice sheet, where there would be increased scattering of sound as the ray paths encountered the ice.) The bottom was simulated as a 17 meter thick sediment layer with a bottom half space. A sandy bottom type was assumed. Due to the upward refracting characteristics of the Arctic, the bottom type did not play a role in propagation.

The BELLHOP MODEL, which is a Gaussian beam propagation model using coherent addition of ray paths, was used in order to keep the model run time reasonable. The 3.5 kHz source was placed at a depth of ten meters. Figures 32 and

33 are the resulting ray traces with transmission loss (TL) referenced dB re 1 micro Pascal.

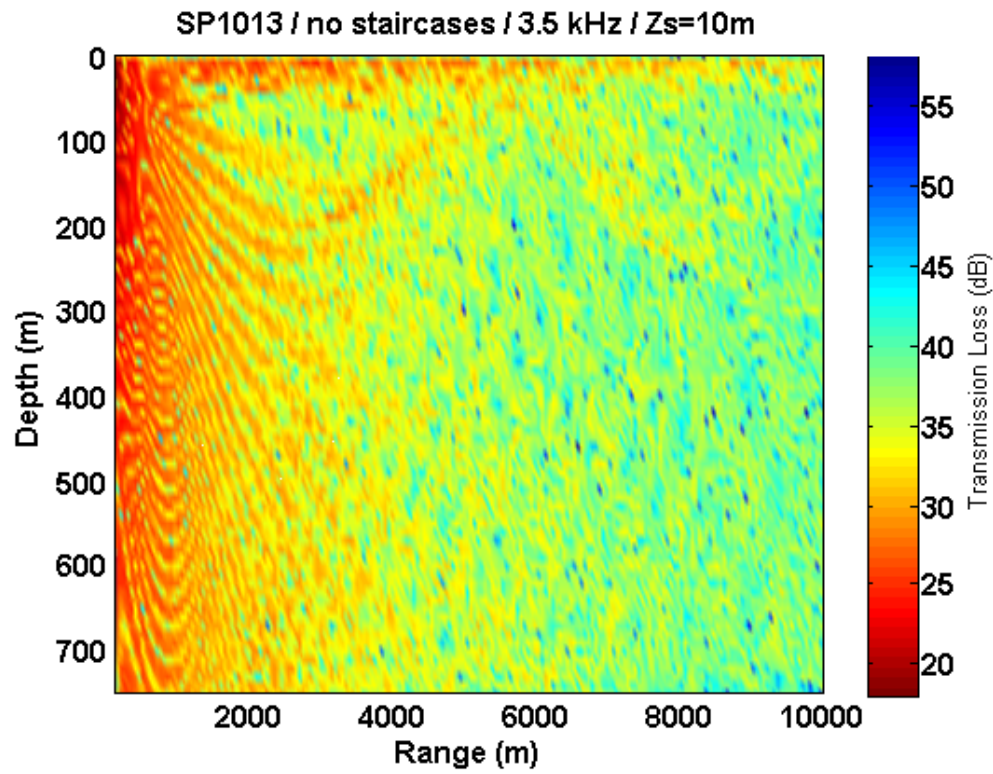


Figure 32. Sound propagation through SVP with no staircases.

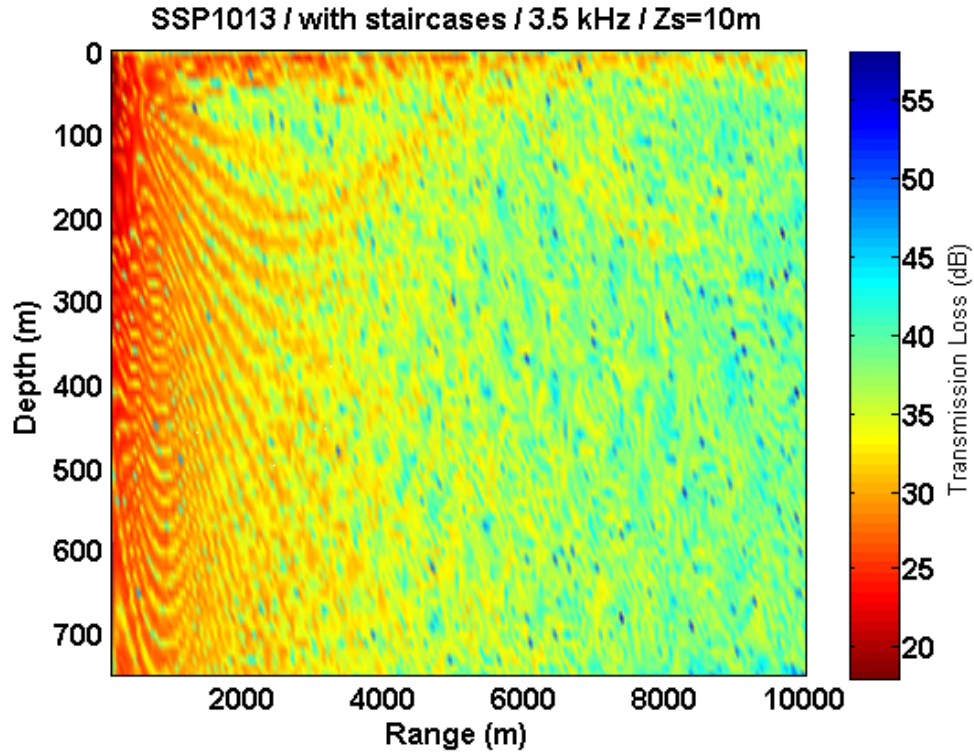


Figure 33. Sound Propagation model through SVP with staircase structure included.

Logarithmic scaling makes it difficult to easily compare the two simulations, so the difference between the two cases is plotted to provide clarity. From Figure 34, it can be determined that within a range of 10000 meters, (range of operational detection), there is a significant impact from the staircases, with differences in TL up to 15 dB. It can be noted that there is very little difference in the ray traces within the first 4000 meters. This is an expected result because in order for the staircases to have an impact, the sound has to be refracted so that it encounters the staircases at near-horizontal angles (a reasonable assumption for any source placement above the staircases because of upward refraction) The difference in TL using this idealized model is between -15 and 15 dB.

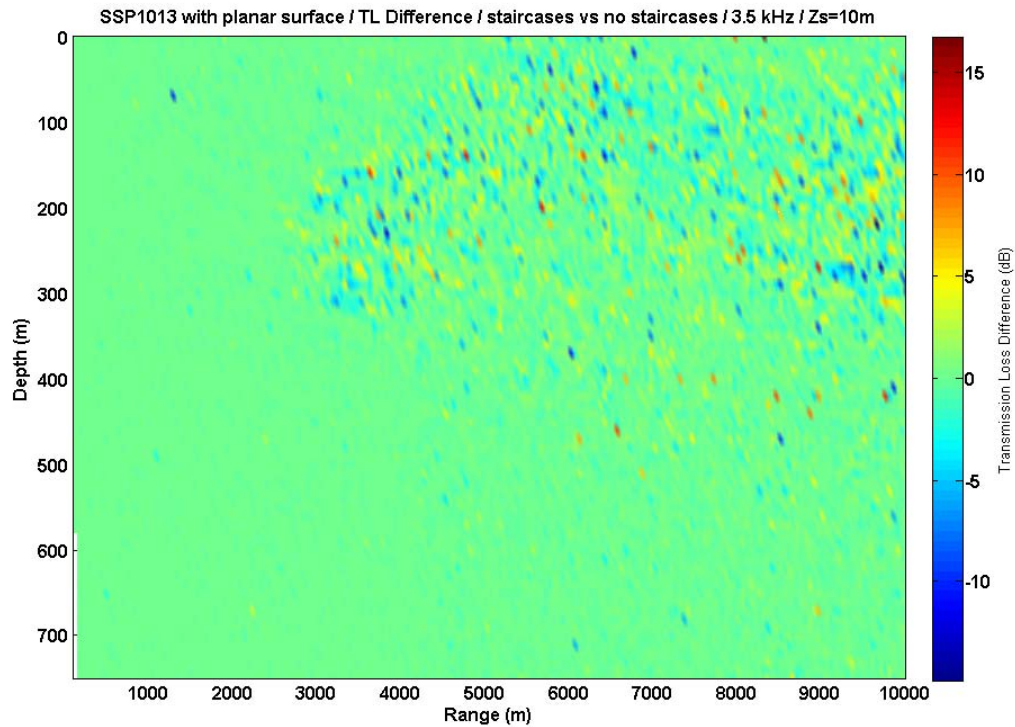


Figure 34. Difference in TL between profiles with and without staircases.

Considering the idealized situation, it is reasonable to assume that scattering from the ice, or other ocean sounds speed structure, could reduce or enhance the range of impact of the staircases. It should be noted that even a 3dB difference can cause a significant impact on detection and should be considered. Further research is needed to realize that full impact of these staircases on sound propagation.

## VI. CONCLUSIONS

Among various aspects of the diffusive convection explored in this study, the most significant was the development of the layer-merging theory for thermohaline staircases. The theory based analysis of the Beaufort Gyre made it possible to evaluate existing flux laws for the ocean. From ice-tethered profiler data, there is evidence that merging follows Radko (2007) B-merger theory. Applying the theory directly to in situ data, it became evident that the pattern of the normalized growth-rate was the same. However, it was determined that the laboratory derived flux laws cannot be directly applied to Arctic staircases. A coefficient is necessary to convert from laboratory to the ocean. The coefficient is determined by analyzing the merging pattern of diffusive layers, and relating it to theory based flux laws. The proposed theoretical model of layer merging events is consistent with the field data.

Based on this consistency, a coefficient "A"  $O(1)$  can be determined and applied to better correlate laboratory flux laws with ocean data. Using different expressions for the  $R_\rho$  dependent coefficient of the  $4/3$  flux law (Kelley, 1990; Marmorino, 1976), we estimate that the average flux from the thermohaline staircases is from  $1-6 \text{ Wm}^{-2}$ . This range of fluxes is significantly higher than if the original  $4/3$  flux law is applied. Inconsistencies in the results of laboratory-derived fluxes provide significant room for error in direct extrapolation to the ocean. Therefore, the higher fluxes derived through merging theory cannot be discounted.

Fluxes in the Arctic are currently of great concern. As Turner and Veronis (2004) suggest through their laboratory experimentation on ice melt, double-diffusive processes may be somewhat responsible for melting Arctic ice. While it has been suggested that fluxes in the Beaufort Gyre staircases cannot penetrate the halocline, it is entirely possible that regions of double-diffusive convection, where the halocline is weaker, could have a greater effect. It is also noted that the heat budget for the Arctic has approximately 1/3 of its fluxes not accounted for by solar input (Perovich et al. 2001). While evidence is inconclusive as to the exact contribution of convective diffusive fluxes to mixed layer over-all flux, it would be negligent not to consider the possibility of its contribution.

In the cycle of global climate change, attention is once again being diverted to the Arctic. The accessibility of resources and shipping routes that a melted ice cap would provide necessitate an operational focus on the impact of microstructures on sound propagation. An idealized propagation model was used to determine whether or not further research was necessary, and found that under normal operational conditions, there was an impact from the staircase structure of up to 30dB. While further research could increase or decrease this magnitude, the difference in transmission loss should be considered in future Arctic operations, and should be further studied to determine the actual magnitude of impact from this structure.

## LIST OF REFERENCES

- Chin-Bing, S. A., King, D. B., & Boyd, J. D. (1994) The Effects of Ocean Environmental Variability on Underwater Acoustic Propagation Forecasting. In Robinson, A. & Lee, D., *Oceanography and Acoustics Prediction and Propagation Models* (24-49). New York: American Institute of Physics.
- Crapper, P. F. (1975). Measurements across a diffusive interface. *Deep-Sea Research*, **22**, 537-545.
- Del Grosso, V. A. (1974). New equation for the speed of sound in natural waters (with comparisons to other equations). *Journal of the Acoustical Society of America* **56(4)**, 1084-1091.
- Fernando, H. J. S. (1987). The formation of layered structure when a stable salinity gradient is heated from below. *Journal of Fluid Mechanics*, **182** (425-442), 525-541.
- Huppert, H. E. (1971). On the stability of a series of double-diffusive layers. *Deep Sea Research*, **18**, 1005-1021.
- Johnson, G. C., Toole, J. M., & Larson, N. G. (2007). Sensor corrections for Sea-Bird SBE-41Cp and SBE-41 CTDs. *Journal of Atmospheric and Oceanic Technology*, **24**, 1117-1130.
- Kelley, D. E. (1988). Explaining effective diffusivities within diffusive oceanic staircases. In J. C. J. Nihoul, & B.M. Jamart (Eds.), *Small-scale turbulence and mixing in the ocean* (481-502). Amsterdam: Elsevier.
- Kelley, D. E. (1990). Fluxes through diffusive staircases: a new formulation. *Journal of Geophysical Research*, **95**, 3365-3371.
- Kelley, D. E., Fernando, H. J. S., Gargett, A. E., Tanny, J. & Ozsoy, E. (2003). The diffusive regime of double-diffusive convection. *Progress in Oceanography*. **56**, 461-481.

- Krishfield, R., & Coauthors (2006): Design and operation of automated Ice-Tethered Profilers for real-time seawater observations in the polar oceans. Woods Hole Oceanographic Institution Tech. Rep. WHOI-2006-NN, 30 pp. <http://hdl.handle.net/1912/1170>, accessed September 12, 2007.
- Marmorino, G. O. & D. R. Caldwell (1976). Heat and salt transport through a diffusive thermohaline interface. *Deep-Sea Research*, **23**, 59-67.
- Padman L. & Dillon, T. M. (1987). Vertical heat fluxes through the Beaufort Sea thermohaline staircase. *Journal of Geophysical Research*, **92 (C10)**, 10799-10806.
- Perovich, D. K., Grenfell, T. C., Richter-Menge, J. A., Light, B., Tucker, W. B., & Eicken, H. (2003). Thin and thinner: Sea ice mass balance measurements during SHEBA. *Journal of Geophysical Research*, **108(C3)**, 1-21.
- Radko, T. (2005). What determines the thickness of layers in a thermohaline staircase? *Journal of Fluid Mechanics*, **523**, 79-98.
- Radko, T. (2007). Mechanics of merging events for a series of layers in a stratified turbulent fluid. *Journal of Fluid Mechanics*, **000**, 1-23.
- Stommel, H., Arons, A. B., & Blanchard, D. (1956). An oceanographical curiosity: the perpetual salt fountain. *Deep-Sea Research*, **3**, 152-153.
- Stern, M. E. (1960). The 'salt fountain' and thermohaline convection. *Tellus*, **12**, 172-175.
- Turner, J. S. (1965). The coupled turbulent transports of salt and heat across a sharp density interface. *International Journal of Heat and Mass Transport*, **8**, 759-767.
- Turner, J. S. & Veronis, G. (2004). The influence of double-diffusive processes on the melting of ice in the Arctic Ocean: laboratory analogue experiments and their interpretation. *Journal of Marine Systems*, **45**, 21-37.

Turner, J. S. (1968). The behavior of a stable salinity gradient heated from below. *Journal of Fluid Mechanics*, **33**, 183-200.

Turner, J. S. (1973) *Buoyancy Effects in Fluids*. New York: Cambridge University Press.

THIS PAGE INTENTIONALLY LEFT BLANK

## INITIAL DISTRIBUTION LIST

1. Defense Technical Information Center  
Ft. Belvoir, Virginia
2. Dudley Knox Library  
Naval Postgraduate School  
Monterey, California
3. Dr. Mary Batteen  
Naval Postgraduate School  
Monterey, California
4. Dr. Timour Radko  
Naval Postgraduate School  
Monterey, California
5. Commander Ben Reeder, United States Navy  
Naval Postgraduate School  
Monterey, California